NASA TECHNICAL MEMORANDUM

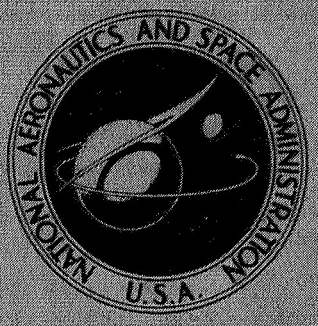

NASA TM X-1787

NASA TM X-1787

MEASUREMENTS OF MUTUAL INTERFERENCE HEATING FOR A PROBE ANTENNA MOUNTED ON AN APOLLO REENTRY CONFIGURATION

by Robert A. Jones and James L. Hunt

Langley Research Center
Langley Station, Hampton, Va.

NATIONAL AERONAUTICS AND SPACE ADMINISTRATION • WASHINGTON, D. C. • JUNE 1969

NASA TM X-1787

MEASUREMENTS OF MUTUAL INTERFERENCE HEATING FOR A PROBE ANTENNA MOUNTED ON AN APOLLO REENTRY CONFIGURATION

By Robert A. Jones and James L. Hunt

Langley Research Center
Langley Station, Hampton, Va.

NATIONAL AERONAUTICS AND SPACE ADMINISTRATION

For sale by the Clearinghouse for Federal Scientific and Technical Information
Springfield, Virginia 22151 – CFSTI price $3.00

MEASUREMENTS OF MUTUAL INTERFERENCE HEATING FOR A PROBE ANTENNA MOUNTED ON AN APOLLO REENTRY CONFIGURATION

By Robert A. Jones and James L. Hunt
Langley Research Center

SUMMARY

A study was made at a Mach number of 8 to determine the interference heating effects of a probe antenna located on the windward afterbody of an Apollo model at a 25° angle of attack and protruding ahead of the undisturbed main bow shock. The interference heating effects were observed to occur only on the windward part of the afterbody. The presence of the probe antenna resulted in peak heating rates as large as 23 times the local value for a model without a probe or 2.3 times the reference heat-transfer coefficient, which was the calculated heat transfer at the stagnation point of the Apollo model at an angle of attack of 0°. This interference heating to the afterbody was very sensitive to Reynolds number with the highest heating rates occurring at the highest Reynolds numbers. The maximum interference heating rates to the probe occurred at the point where the slip-flow line emanating from the intersection of the body bow shock and the probe shock impinged on the lower edge of the probe. The value of this maximum heat-transfer rate to the probe was 15.5 times the reference value or 1.3 times the estimated value for the probe leading edge subjected to the undisturbed local flow conditions immediately behind the body bow shock.

INTRODUCTION

A study has been made at the Langley Research Center to determine the feasibility of using a probe antenna as a means for providing continuous communication during reentry of the Apollo command module at velocities of about 11 000 m/sec. A discussion of the probe antenna as a method for alleviating communication blackout is given in references 1 and 2. The basic concept is to locate an antenna within a small slender probe which is placed ahead of the large blunt shock enveloping the main body. The radio signal from such an antenna would have to penetrate a much thinner, less dense, lower temperature plasma than the one surrounding the main body, and thus the possibility of achieving continuous communication during reentry would be increased. Wind-tunnel tests have established that the probe antenna has a small effect on the aerodynamic

stability of the spacecraft. (See ref. 3.) Another problem encountered with such a probe antenna is the effect of the mutual interference of the probe flow field and that of the main body on the heat-transfer rate to the body and to the probe. The purpose of the investigation reported herein was to determine the magnitude of these interference heating effects and to provide a basis for the selection of a probe geometry which would give minimum interference heating.

For this interference heating study, certain basic requirements are assumed. The primary requirements which affect this investigation are

(1) The antenna itself must be conical in shape, approximately 39.37 cm long for a full-scale Apollo configuration, and must be located so as to always be forward of the undisturbed main bow shock of the body.

(2) The antenna support strut must be attached to the Apollo vehicle at the Block II umbilical door, which is on the windward afterbody ray just downstream of the corner.

(3) The strut must be designed to allow for structure and heat shielding that would insure survival of the probe antenna during the Apollo reentry at velocities of 10 972.8 m/sec.

The investigation consisted of several different phases. In the first phase the shock shape about the Apollo body was determined at conditions which represented the maximum and minimum shock standoff distances for a reentry velocity of 10 972.8 m/sec and conditions where communication blackout was likely to occur. Second, preliminary tests of 39 different probe configurations all supported from the umbilical door location were made and the interference heating to the body was measured. Third, detailed interference heating distributions were measured on the Apollo afterbody for the probe-antenna configuration which was thought to be the most feasible. Finally, measurements of heating rates to the probe itself were made for one probe configuration.

The shock shape for the minimum shock standoff distance was measured in a small hypersonic tunnel by using tetrafluoromethane (CF_4) as the test gas to obtain high normal-shock density ratios. All other tests were made in the Langley Mach 8 variable-density tunnel. Coatings of fusible temperature indicators were used to measure heat-transfer rates.

SYMBOLS

a — length of probe extending beyond model (fig. 2)

b — height of probe above model (fig. 2)

c	position of strut on afterbody (fig. 2)
D	model face diameter
h	measured local heat-transfer coefficient
h_o	reference heat-transfer coefficient (calculated value at the stagnation point for an angle of attack of 0^o)
M_∞	free-stream Mach number
$R_{\infty,D}$	free-stream Reynolds number based on model face diameter
r	radius
r_c	corner radius of model
r_n	nose radius of model
$r_{n,eff}$	effective nose radius of model
θ	strut sweep angle (fig. 2)
ρ_2	density of gas behind normal shock wave
ρ_∞	free-stream density of gas

FACILITIES

Tests were made in a small pilot model hypersonic CF_4 blowdown tunnel at the Langley Research Center in which a good simulation of the forebody shock shapes at the high normal-shock density ratios encountered in flight could be obtained. Tests were conducted at a stagnation pressure of about 1.034×10^7 N/m^2 with a stagnation temperature of 422^o K. The simulated free-stream Mach number and normal-shock density ratio were 7.5 and 12, respectively. This facility and the degree of simulation of forebody flow fields that can be achieved with CF_4 as the test gas are described in detail in reference 4. All other tests were made in the Langley Mach 8 variable-density tunnel which is described in reference 5. The stagnation pressure in this facility was varied over a range from 6.895×10^5 to 3.551×10^6 N/m^2 with stagnation temperatures ranging from 700^o to 755^o K.

MODELS

It was desirable to use as large a model as could be tested in the facility; therefore, a 2/77-scale model of the Apollo command module was used. A sketch of this basic model is shown in figure 1. This model was made of high-temperature plastic so that data could be obtained by using the fusible temperature indicator (ref. 6). The preliminary tests were made with probes constructed of 0.159-cm-diameter steel rods shaped into various configurations and cemented into holes in the afterbody of the basic model. The geometry of the different probes tested is given in figure 2. A total of 39 different probe configurations were tested in this preliminary series. The half-angle of the probe tip was 8°. The different fairings shown in figure 2 were made by adding solder to the 0.159-cm-diameter rod and filing it to the desired shape.

A drawing and photograph of the final probe-antenna configuration are presented in figure 3. This probe was handmade from aluminum. A small ramp which was placed just upstream of the base of the probe for several tests is shown in figure 4. This ramp was made from the same plastic material as the basic model. It was 1.27 cm wide, about 1.11 cm long, and had a taper of 8° so that its top surface was parallel to the free-stream flow for an angle of attack of 25° (near trim angle of attack).

A two-dimensional model, shown in figure 5, was used to measure heat transfer to the probe itself.

TEST TECHNIQUE

Heat-transfer data were obtained by a fusible-temperature-indicator technique described in reference 6. In this technique the heat-transfer coefficients are determined by measuring the time required for a point on the surface of the model to reach the phase-change temperature of the thin fusible coating, as determined visually. These values of time and temperature are then used in the solution to the heat conduction equation for a semi-infinite slab with a step input in h to ascertain the heat-transfer coefficient. The phase-change patterns are recorded by motion-picture photography. The negatives are projected onto a screen, and a sketch of the model as well as lines representing the phase-change pattern is drawn. The line for each phase-change pattern is a line of constant heat-transfer coefficient provided the adiabatic wall temperature is constant.

RESULTS AND DISCUSSION

Shock Shape Studies

One of the assumptions made for this study was that in order to achieve transmission the antenna itself would be conical in shape with a half-angle of about 8° and a length of about 39.37 cm for the full-scale Apollo. (See refs. 1 and 2.) The center line of the antenna was to be alined parallel to the free-stream flow for an angle of attack of 25° and the antenna was to be located so that its full length would be in front of the bow shock from the basic Apollo body. For flight at conditions where communication blackout may be expected, the density ratio across the body bow shock, and therefore the shock location relative to the body, varies considerably because of different degrees of dissociation in the shock layer. It was necessary then to determine the maximum variation in bow shock locations relative to the basic body so that the probe could be properly positioned to insure that the antenna would clear the undisturbed main body bow shock. This determination was made by taking schlieren photographs in the Mach 8 tunnel in air where the density ratio across a normal shock was 5.6 and in a pilot CF_4 tunnel where the density ratio across a normal shock was 12.1. Sample photographs of these flows are given in figures 6(a) and 6(b). It was assumed that the most forward shock location corresponded to that observed for the model tested in the Mach 8 tunnel in air and the most rearward shock location to that for the model tested in the CF_4 tunnel. All the probes tested were designed so as to have the entire antenna ahead of the shock for the Mach 8 test conditions. The CF_4 shock shape was used to determine the area on the probe where maximum interference heating due to the impingement of the strong bow shock from the basic body would occur under flight conditions.

Measurement of heat-transfer rates to the probe itself required a larger probe than the 2/77-scale probes used on the Apollo model. In order to simulate the effects of the strong bow shock impingement on the probe and the effects of the flow expansion around the windward corner of the Apollo shape on the heat transfer to the probe and at the same time use a larger probe than one that could be placed on a scale model of the Apollo, a two-dimensional model was used. A sketch of this two-dimensional model is shown in figure 5, and a schlieren taken of the model without a probe in the Mach 8 tunnel is shown in figure 6(c). The shock standoff distance for this two-dimensional model is much greater than that for the windward corner of the Apollo model; therefore, the probe for the two-dimensional model could be made three times as large as the probes used to get interference heating to the basic Apollo body.

Interference Heating to the Command Module

Preliminary probe configurations.- In order to study the effects of various probe geometries such as height, length, location on main body, et cetera, on interference heating to the basic body and to determine a probe geometry which would give minimum interference heating to the command module, preliminary tests were made. No measurements of heating to the probe were made in these preliminary tests. A total of 39 different probe configurations as shown in figure 2 were tested. All these tests were made with the basic Apollo model at a 25° angle of attack, at a stagnation pressure of about 1.48×10^6 N/m^2, and at a stagnation temperature of about 755° K. The fusible temperature indicator used had a phase-change temperature of 325° K. These conditions resulted in a free-stream Reynolds number of 0.33×10^6 based on model face diameter and a ratio of wall to stagnation temperature of 0.43.

Samples of the heat-transfer results on the windward afterbody of the Apollo model for 10 different probe configurations are shown in figure 7. The data are given as the nondimensional ratio h/h_o where h is the measured local heat-transfer coefficient and h_o is a reference heat-transfer coefficient taken to be the calculated value at the stagnation point of the basic Apollo model for an angle of attack of 0° under identical flow conditions. The method used to calculate this reference value is explained in reference 7. Measured heat-transfer rates to the clean (no probe) Apollo afterbody in the same test facility at similar test conditions are also shown in reference 7. For an angle of attack of 25° the value of h/h_o for the clean afterbody was approximately 0.10 for the entire windward part of the afterbody. Depending on probe geometry, the maximum value of h/h_o varied from a low of 0.23 to a high of 0.50 because of interference from the probe antenna. (See fig. 7.) Thus the presence of the probe antenna resulted in heating rates as large as five times those of a clean Apollo model. For all of the preliminary tests the increases in heating due to the presence of the probe antenna were confined to the afterbody. The corner of the afterbody at approximately the tangent point of the surface and the free-stream flow was the most forward location to experience a heating increase.

The effect of varying the strut sweep angle θ on interference heating to the afterbody can be seen by comparing figures 7(a) with 7(b) and 7(c) with 7(d). In figures 7(a) and 7(b) the probe geometry is the same except for the angle θ which is 45° and 90°, respectively. For the more highly swept configuration of figure 7(a), a lower peak heating rate to the afterbody and a smaller area subjected to interference heating occurred. For the longer probe (figs. 7(c) and 7(d)), the same sweep-angle effects were obtained.

The effect of probe height b on interference heating to the afterbody can be seen by comparing figures 7(a) and 7(e). The two configurations in these figures are the same except that the probe height b was 0.635 cm for the model in figure 7(a) and 1.02 cm

for the model in figure 7(e). The comparison indicates that the lower probe resulted in less interference heating to the afterbody.

The effect of the probe length a on the interference heating to the afterbody can be seen by comparing figure 7(a) with 7(c), 7(b) with 7(d), and 7(h) with 7(i). The area on the afterbody which was subjected to the higher interference heating was slightly larger for the longer probe when the strut leading edge was blunt (see figs. 7(a), 7(c), and 7(b) and 7(d)). However, there was no noticeable increase in the interference heating area with a change in probe length when the strut had a sharp leading edge (figs. 7(h) and 7(i)). In general the sharp leading-edge strut was often better than the blunt leading-edge strut since it resulted in less interference heating or a smaller interference heating area. In no case was the sharp strut observed to give more interference than the blunt strut (see, for example, figs. 7(f) and 7(g)).

The effect of the fore and aft position of the strut on the afterbody c can be seen by comparing figures 7(b) and 7(f). The more forward location (fig. 7(b)) resulted in a slightly larger area subject to the high interference heating, but this effect may be partially offset by the lower weight associated with the shorter length probe at the more forward position.

The effects of several different type fillets in the region of the probe-strut juncture (see fig. 2(b)) on the interference heating to the afterbody were also studied. An example which is typical of the results obtained with a fillet present is shown in figure 7(j). When the data for the models in figures 7(a) and 7(j), which were similar except for the fillet, were compared, the maximum interference heating was found to be about the same for each model; however, for the model with the fillet, a somewhat larger area on the afterbody was subjected to moderate interference heating rates ($0.14 \leq h/h_o \leq 0.23$).

Final-probe configuration.- Based on the results of the preliminary heat-transfer tests and consideration of structural and heat-shielding estimates, a probe-antenna configuration thought to be feasible for an Apollo configuration was selected. A sketch and photograph of this probe-antenna configuration is shown in figure 3. The circular cross section of this probe at station A-A has a diameter about twice that of the preliminary probes. The larger size was necessary in order to contain the structure and heat shielding required to adequately protect and support the probe during reentry.

The measured interference heating rates to the afterbody with the final probe-antenna configuration are shown in figure 8 along with sample photographs of the phase-change patterns and a schlieren photograph of the flow. These data were taken at a free-stream Reynolds number of 0.33×10^6 based on model face diameter. The interference heating with this probe antenna was confined to the afterbody as was that for the preliminary probes. However, the maximum measured interference heating rate h/h_o was 1.20,

which was approximately 2.4 times the maximum value for the preliminary probes. This increase was probably due to the much larger cross-sectional area of the final probe antenna. Furthermore, the area subjected to interference heating was larger than that of the preliminary configurations. The data for other Reynolds numbers (fig. 9) indicate a large increase in interference heating rate with an increase in Reynolds number. The maximum interference heating rate was 2.3 for a Reynolds number of 0.51×10^6 based on model face diameter.

A small ramp (fig. 4) was placed just ahead of the strut in an attempt to reduce the high interference heating rates to the afterbody. The results with this ramp present are shown in figures 10 and 11. This ramp proved to be very effective in reducing the high heating rates, particularly at the high Reynolds numbers. The peak interference heating rate at the highest Reynolds number was reduced by a factor greater than three (compare fig. 11(b) with 9(b)), but at the lowest Reynolds number, the ramp reduced the heating rate only slightly.

Interference Heating to the Probe Antenna

The probe antenna on the 2/77-scale Apollo model was too small for meaningful measurements of the heat-transfer rate to the probe to be made. Therefore, as previously mentioned, a two-dimensional model was used to approximately simulate the interference flow field over the windward corner of the model. This simulation allowed a larger shock standoff distance and, thus, the use of a larger probe antenna. The shock interference obtained simulated that of a model with a nose radius of 37.08 cm $(r_{n,eff})$. A sketch of the two-dimensional model is shown in figure 5. The face of the model was flat and alined normal to the free-stream flow to give a maximum shock standoff distance. The corner radius was made 2.5 times that of 2/77-scale model, and the afterbody angle was 11^o so as to provide the same expansion angle as for the Apollo model. The probe antenna was 3.04 times as large as the one tested on the 2/77-scale model and had a steel tip to prevent melting during the test.

A schlieren photograph of the flow about the large probe and simulated body is shown in figure 12, and samples of the phase-change patterns on the probe are shown in figure 13. The slip-flow line emanating from the intersection of the body bow shock and the probe shock impinges on the lower edge of the probe at approximately the region of peak heating as determined from the phase-change patterns of figure 13. The measured heat-transfer distribution on the probe is shown in figure 14 for the same stagnation temperature (755^o K) and pressure (3.54×10^6 N/m^2) as the other high Reynolds number data at a Mach number of 8. Because of the larger scale of this probe, the Reynolds number based on free-stream conditions and the face diameter of the simulated Apollo model was 1.53×10^6. The data are nondimensionalized by the calculated heat-transfer coefficient

for the stagnation point of an Apollo model of the same scale as the probe at an angle of attack of 0^{o} (h_{o} = 98.9 W/m^2-^{o}K). The peak interference heating rate shown in figure 14 is 15.5 at the point where the slip-flow line intersects the lower edge of the strut. An estimate of the heat-transfer coefficient to the leading edge of the strut in the region of high interference heating was made. This estimate was based on the assumption that the leading edge was a swept infinite cylinder subject to flow conditions corresponding to the local flow immediately behind the undisturbed bow shock at the point where it would intersect the probe. This estimate was based on the method of reference 8 and gave a value of 1.18×10^3 W/m^2-^{o}K. The measured peak interference heating on the probe (1.532×10^3 W/m^2-^{o}K) was then 30 percent greater than this estimated value for an infinite cylinder having a radius equal to that of the probe's leading edge.

CONCLUSIONS

The results of tests conducted at a Mach number of 8 to determine the interference heating effects of a probe antenna located on the windward afterbody of an Apollo model and protruding ahead of the undisturbed main bow shock are as follows:

1. The presence of the final probe-antenna configuration resulted in heating rates to the afterbody as large as 23 times the local value for a model without a probe or 2.3 times the reference value which was the calculated heat transfer at the stagnation point of the Apollo body at an angle of attack of 0^{o}.

2. The interference heating effects were observed to occur only on the windward part of the afterbody.

3. The interference heating rate to the afterbody was very sensitive to Reynolds numbers with the highest rates occurring at the highest Reynolds numbers.

4. A small ramp located at the base of the probe strut was found to reduce the interference heating rate to the afterbody. The heating rate was reduced by a factor larger than three at the highest Reynolds number, but at the lowest Reynolds number, the reduction was small.

5. The maximum interference heating to the probe occurred at a point where the slip-flow line emanating from the intersection of the body bow shock and the probe shock impinged on the lower edge of the probe. The value of this maximum heat-transfer rate to the probe was 15.5 times the reference value or 1.3 times the estimated value for the

probe leading edge subjected to the undisturbed local flow conditions immediately behind the body bow shock.

Langley Research Center,
National Aeronautics and Space Administration,
Langley Station, Hampton, Va., February 18, 1969,
124-07-02-60-23.

REFERENCES

1. Sims, Theo E.: Communication Through Reentry Plasma. Conference Record – 1966 Winter Convention on Aerospace & Electronic Systems, Vol. I, IEEE, c.1966, pp. IB-21 – IB-28.

2. Sims, T. E.; and Grantham, W. L.: Reentry Plasma Studies. Proceedings of the Conference on the Applications of Plasma Studies to Reentry Vehicle Communications, Vol. II, Avionics Lab., U.S. Air Force, 1967.

3. Putnam, Lawrence E.: Effects of Two Probe Antennas on Aerodynamic Characteristics of Apollo Spacecraft at Mach 10.03. NASA TN D-4034, 1967.

4. Jones, Robert A.; and Hunt, James L.: Use of Tetrafluoromethane to Simulate Real-Gas Effects on the Hypersonic Aerodynamics of Blunt Vehicles. NASA TR R-312, 1969.

5. Stainback, P. Calvin: Heat-Transfer Measurements at a Mach Number of 8 in the Vicinity of a 90° Interior Corner Alined With the Free-Stream Velocity. NASA TN D-2417, 1964.

6. Jones, Robert A.; and Hunt, James L.: Use of Fusible Temperature Indicators for Obtaining Quantitative Aerodynamic Heat-Transfer Data. NASA TR R-230, 1966.

7. Jones, Robert A.: Experimental Investigation of the Overall Pressure Distribution, Flow Field, and Afterbody Heat-Transfer Distribution of an Apollo Reentry Configuration at a Mach Number of 8. NASA TM X-813, 1963.

8. Reshotko, Eli; and Cohen, Clarence B.: Heat Transfer at the Forward Stagnation Point of Blunt Bodies. NACA TN 3513, 1955.

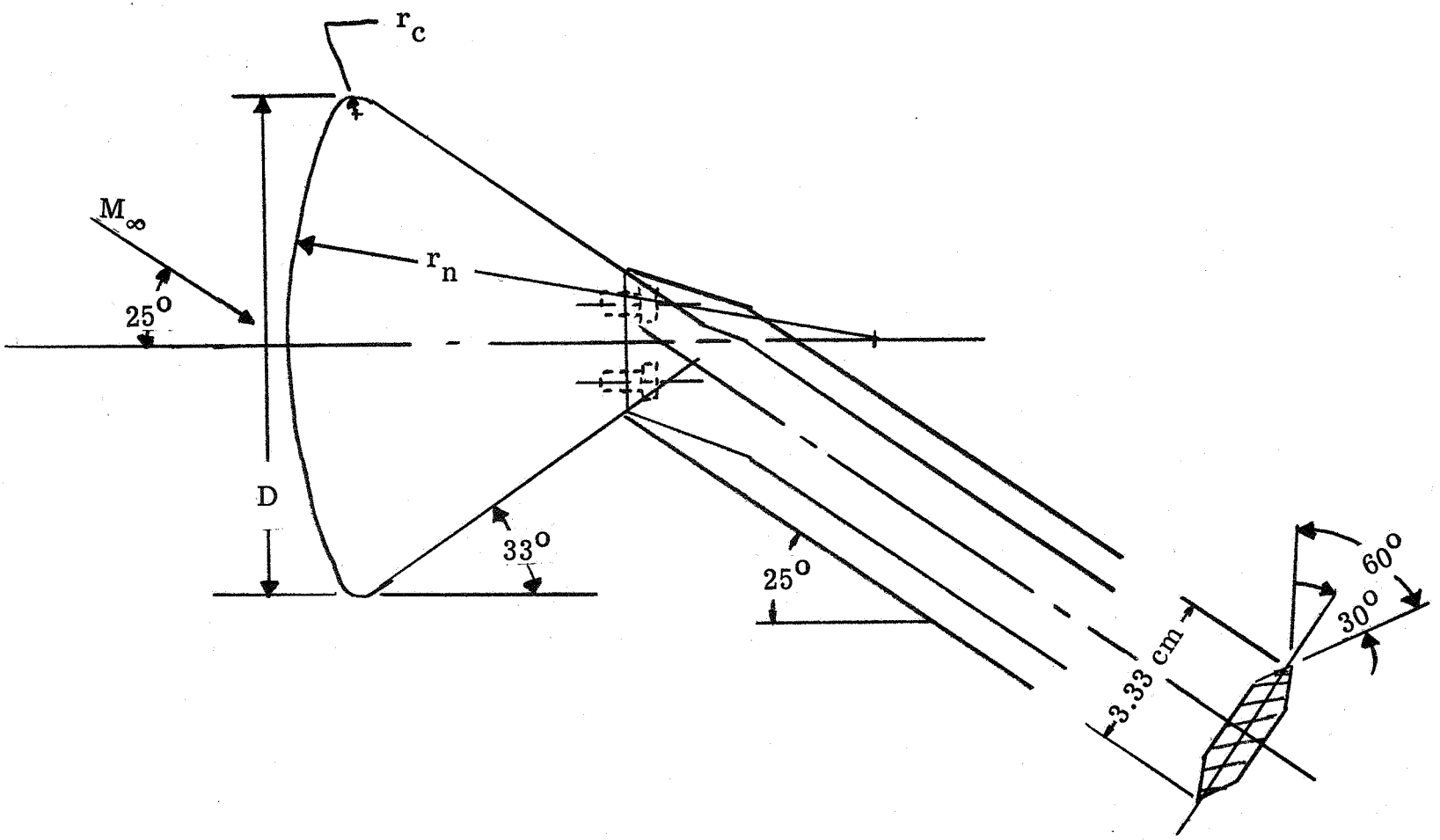

Figure 1.- Sketch of basic model of Apollo command module. D = 10.16 cm; r_n = 1.20D; r_c = 0.05D.

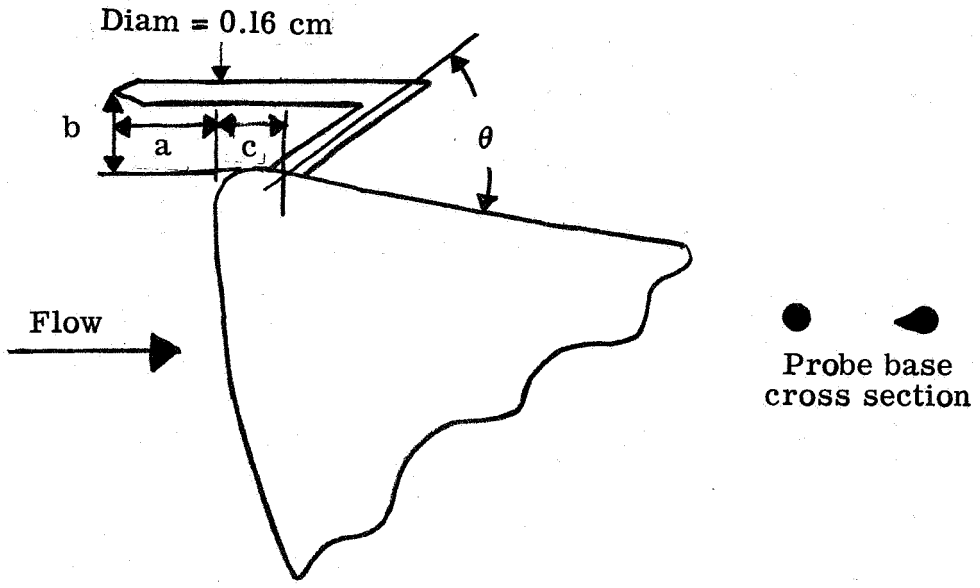

Probe geometry			
a, cm	b, cm	c, cm	θ, deg
1.27	0.635	1.27	45
		1.27	90
		2.03	45
		2.03	90
	1.02	1.27	45
		1.27	90
		2.03	45
		2.03	90
2.38	.635	1.27	45
		1.27	90
		1.27	135
		2.03	45
		2.03	90
	1.02	1.27	45
		1.27	90
		1.27	135
		2.03	45
		2.03	90

(a) Without fillet.

Figure 2.- Preliminary probe-antenna geometry.

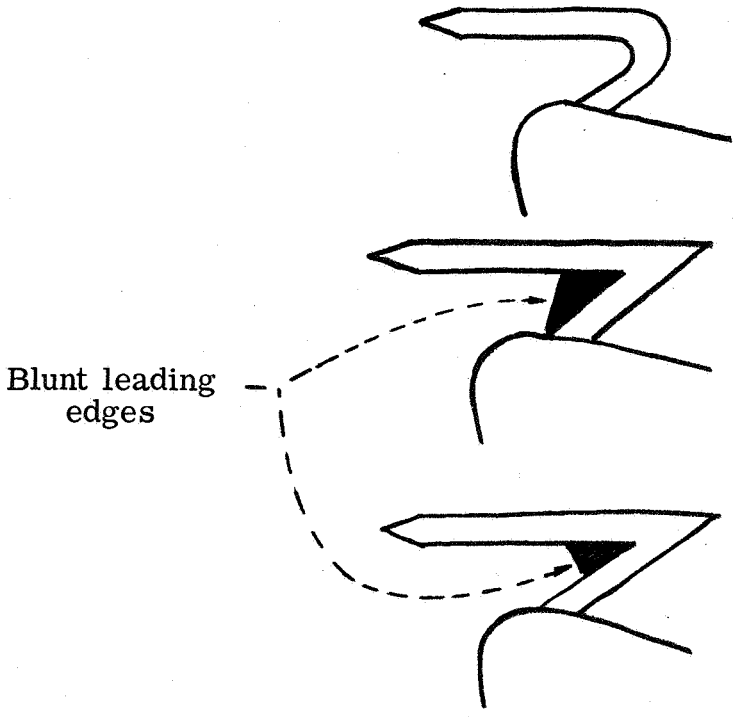

(b) With fillet. a = 1.27 cm; b = 0.635 cm; c = 1.27 cm; $\theta = 45^{0}$.

Figure 2.- Concluded.

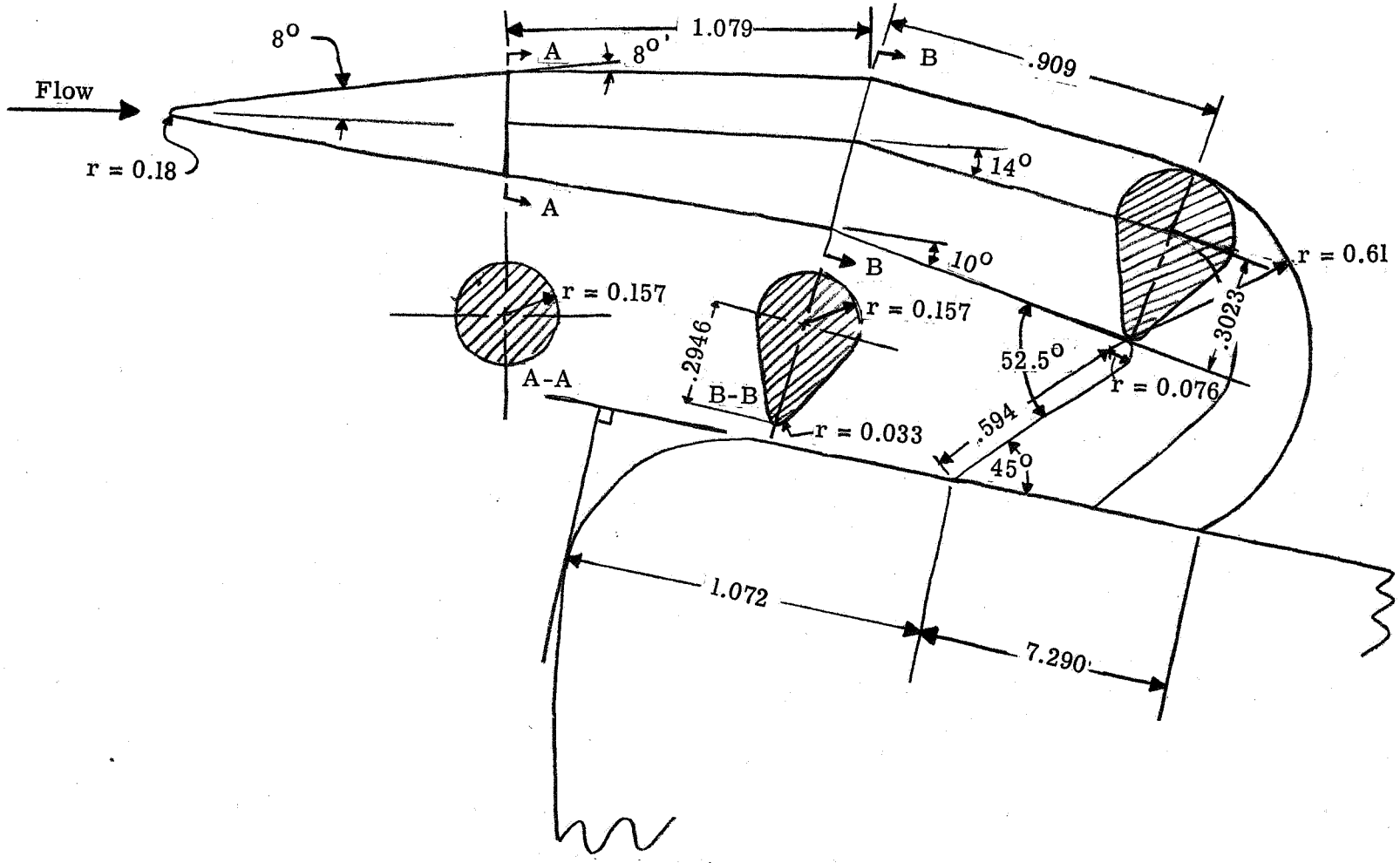

(a) Drawing.

Figure 3.- Final probe-antenna configuration. All linear dimensions are in centimeters.

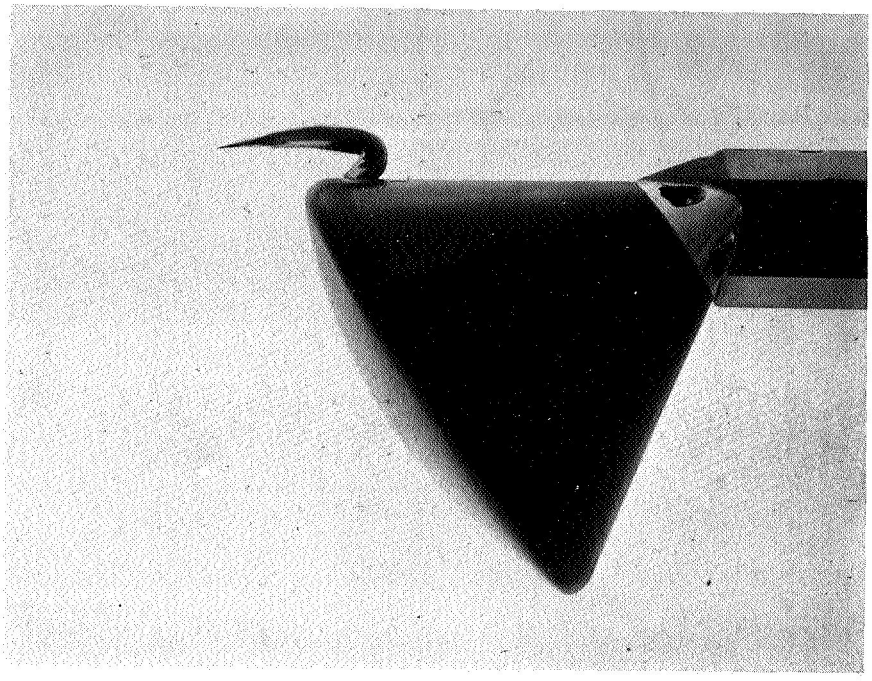

L-69-1239

(b) Photograph.

Figure 3.- Concluded.

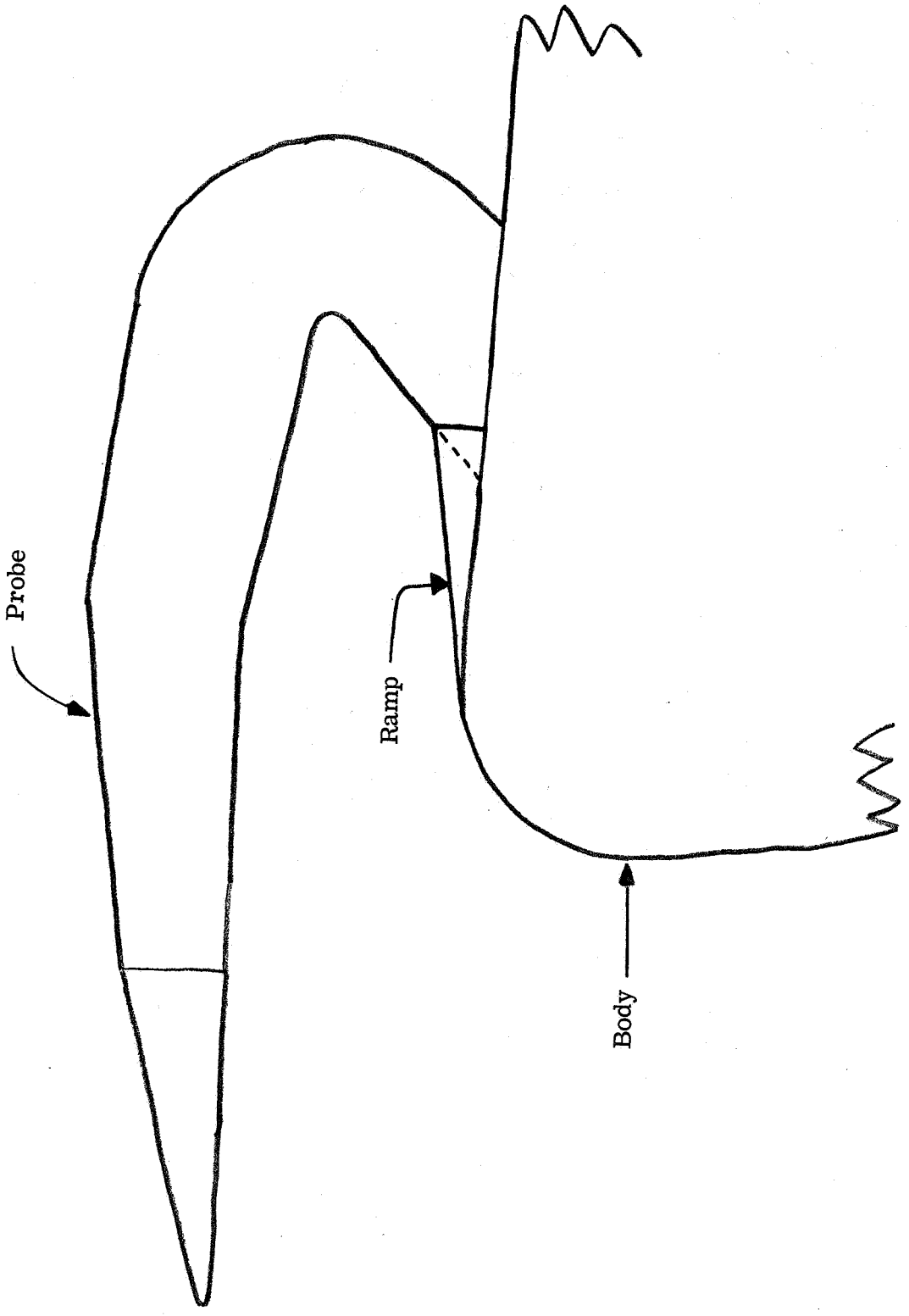

Figure 4.- Ramp location.

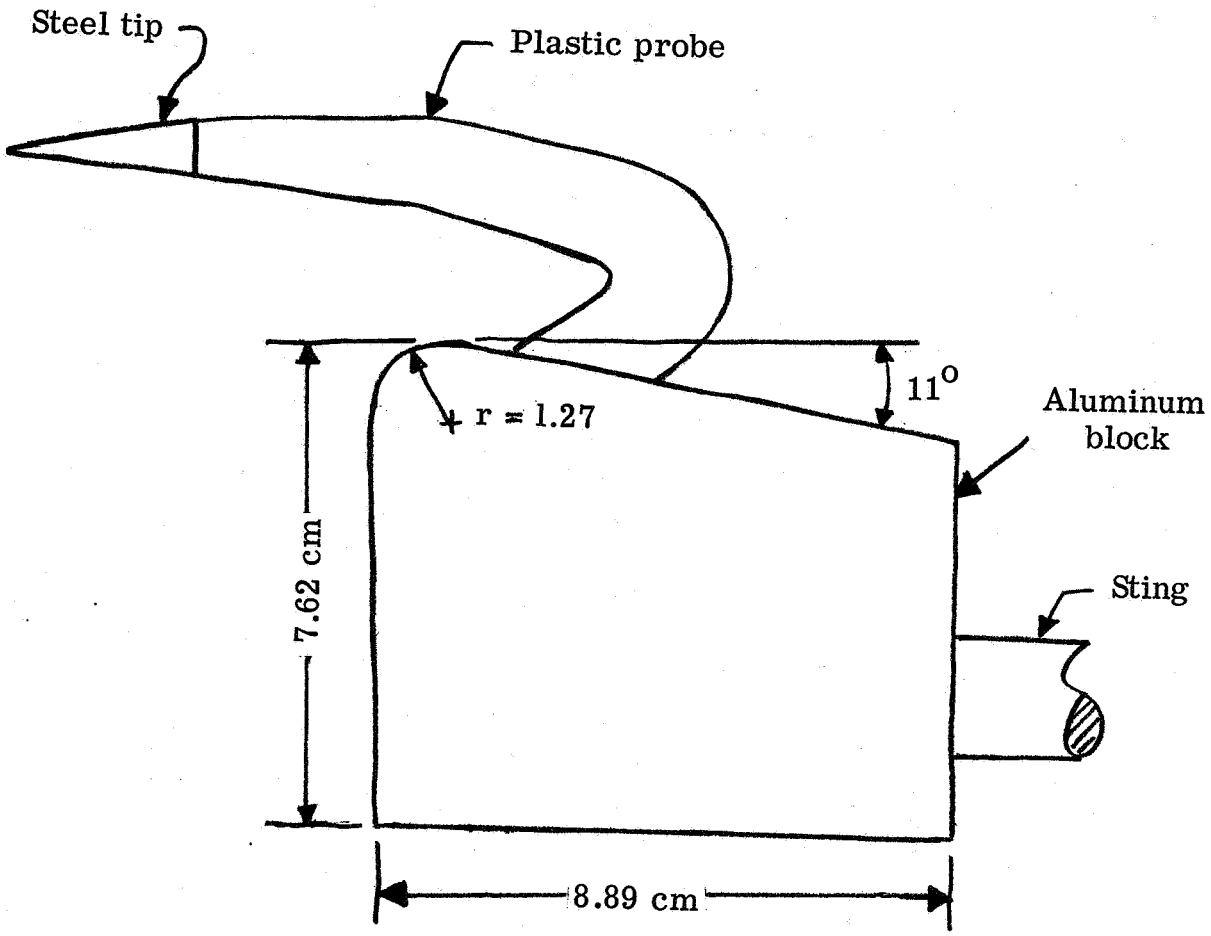

Figure 5.- Cross-sectional view of two-dimensional model. Model width, 20.32 cm.

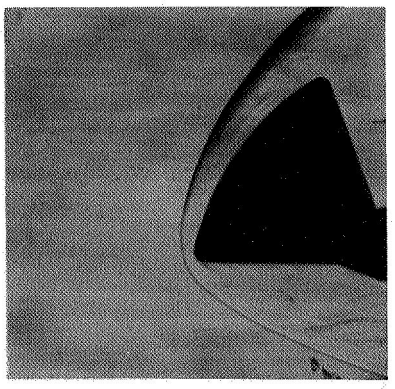

(a) Basic Apollo model in air. $\frac{\rho_2}{\rho_\infty} = 5.6$.

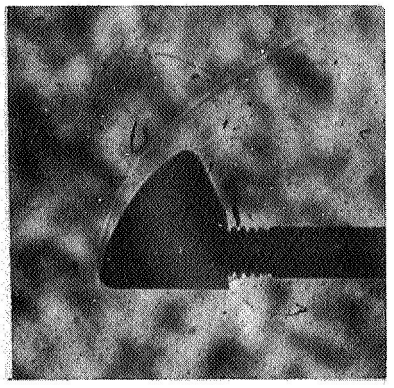

(b) Basic Apollo model in CF_4. $\frac{\rho_2}{\rho_\infty} = 12.1$.

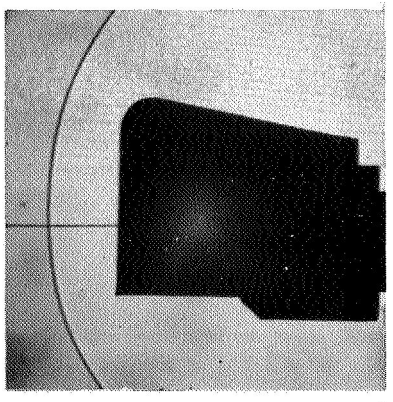

(c) Two-dimensional model in air. $\frac{\rho_2}{\rho_\infty} = 5.6$.

Figure 6.- Shock shapes for basic models. L-69-1240

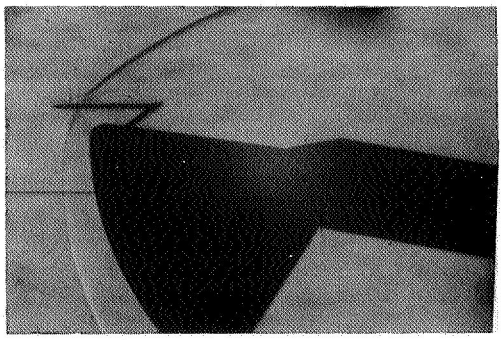

$\frac{h}{h_o}$

0.32 — — — — —
.23 . . . . . .
.18 — · — · — · —
.14 — — · — —
.11 — — · · — — · ·

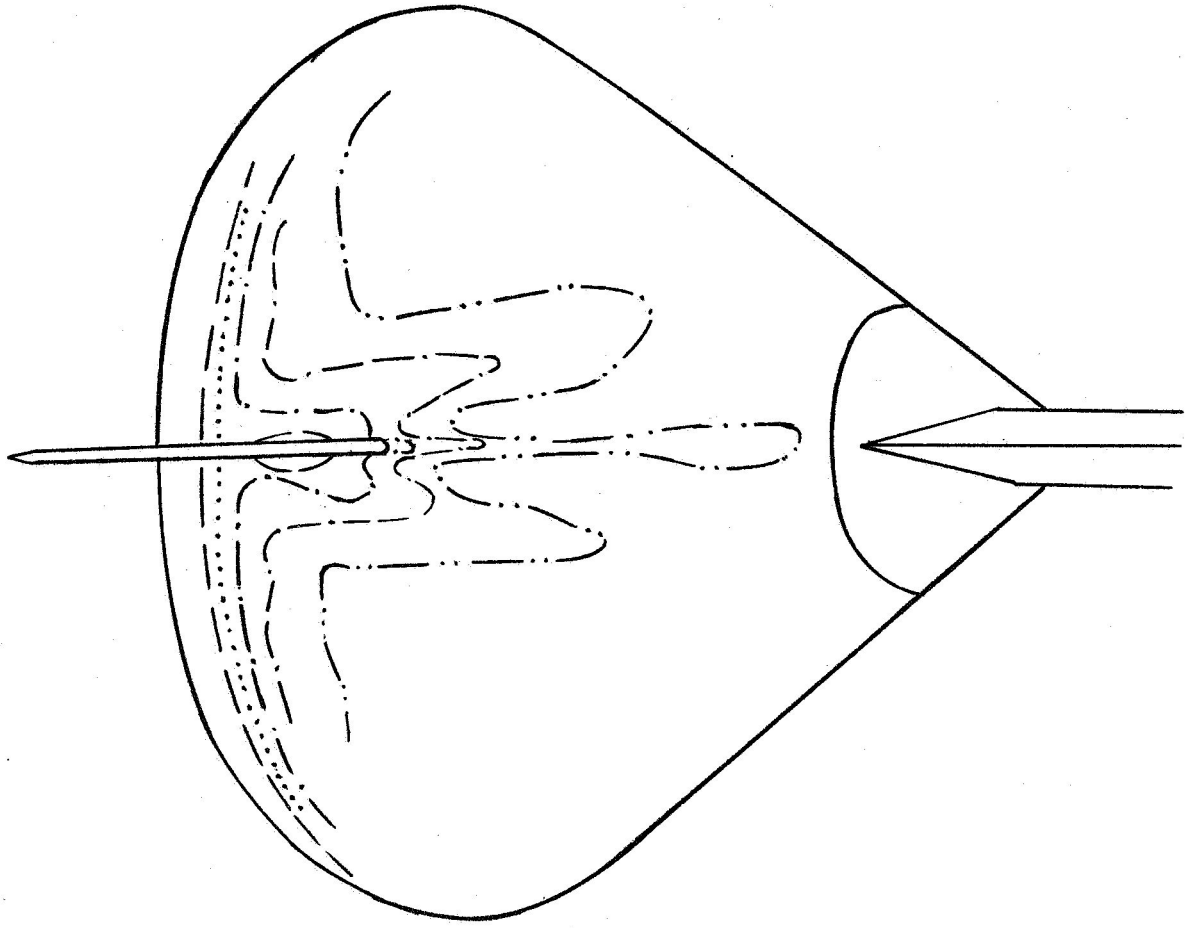

(a) a = 1.27 cm; b = 0.635; c = 1.27 cm; $\theta = 45^{o}$; blunt leading-edge strut. L-69-1241

Figure 7.- Samples of heat-transfer results of preliminary tests on windward afterbody of Apollo model for 10 probe configurations.

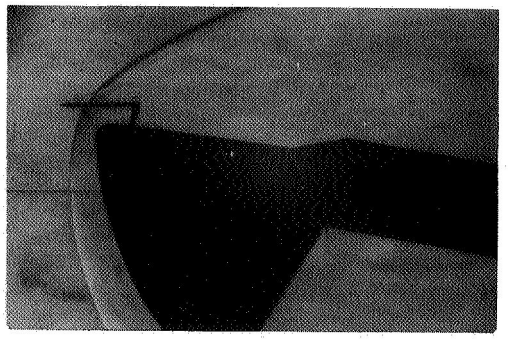

$\frac{h}{h_o}$

0.50 ——————————

.32 — — — — — —

.23 . . . . . .

.18 — · — · — · —

.14 — — · — — · — —

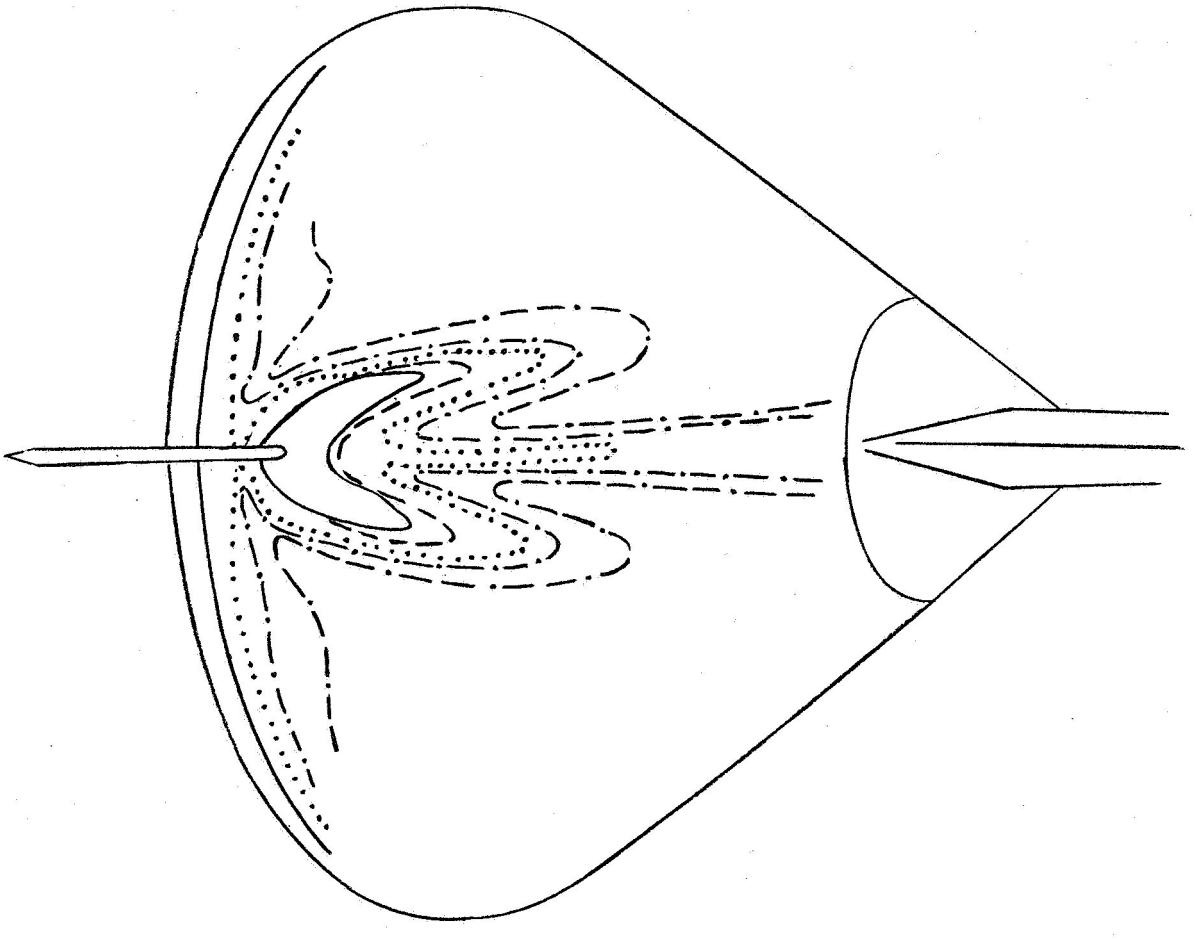

(b) a = 1.27 cm; b = 0.635 cm; c = 1.27 cm; $\theta = 90^{o}$; blunt leading-edge strut.

Figure 7.- Continued.

L-69-1242

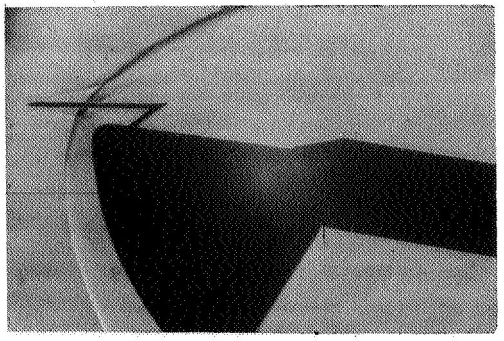

$\frac{h}{h_o}$

0.32 — — — —
.23 . . . . . .
.18 — · — · — ·
.14 — — · — —
.11 — · — · — ·

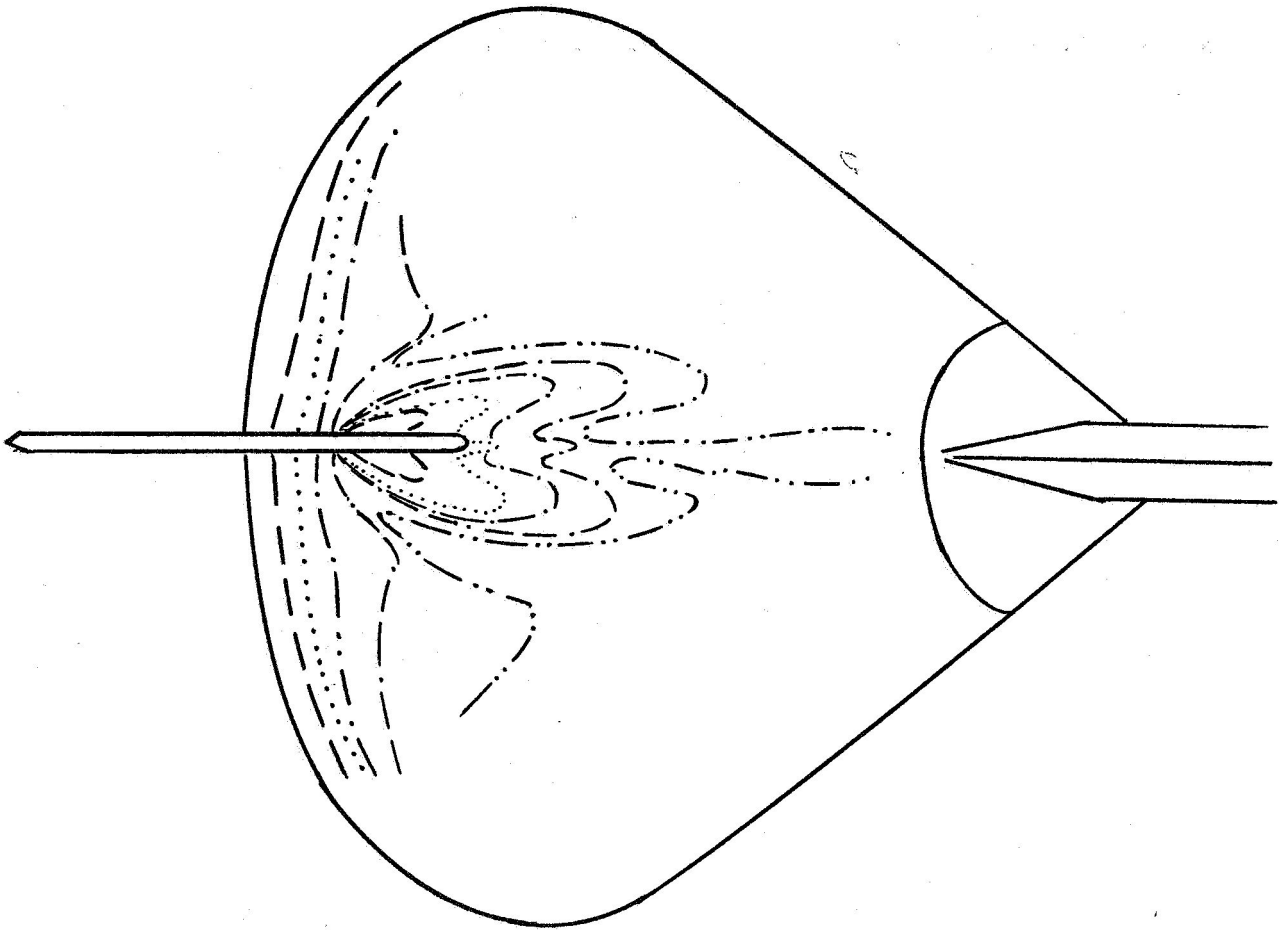

(c) a = 2.39 cm; b = 0.635 cm; c = 1.27 cm; $\theta = 45^{0}$; blunt leading-edge strut.

Figure 7.- Continued.

L-69-1243

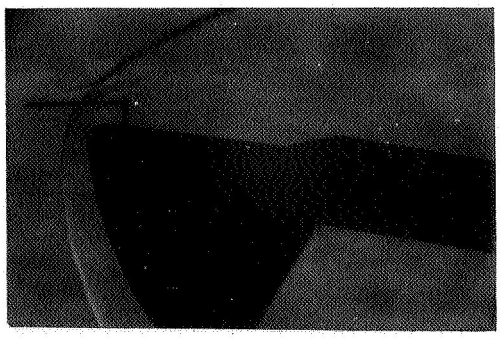

$\frac{h}{h_o}$

0.50 ——————————
.32 — — — — — — —
.23 · · · · · · · · ·
.18 — · — · — · —
.14 — — · — — · — — ·

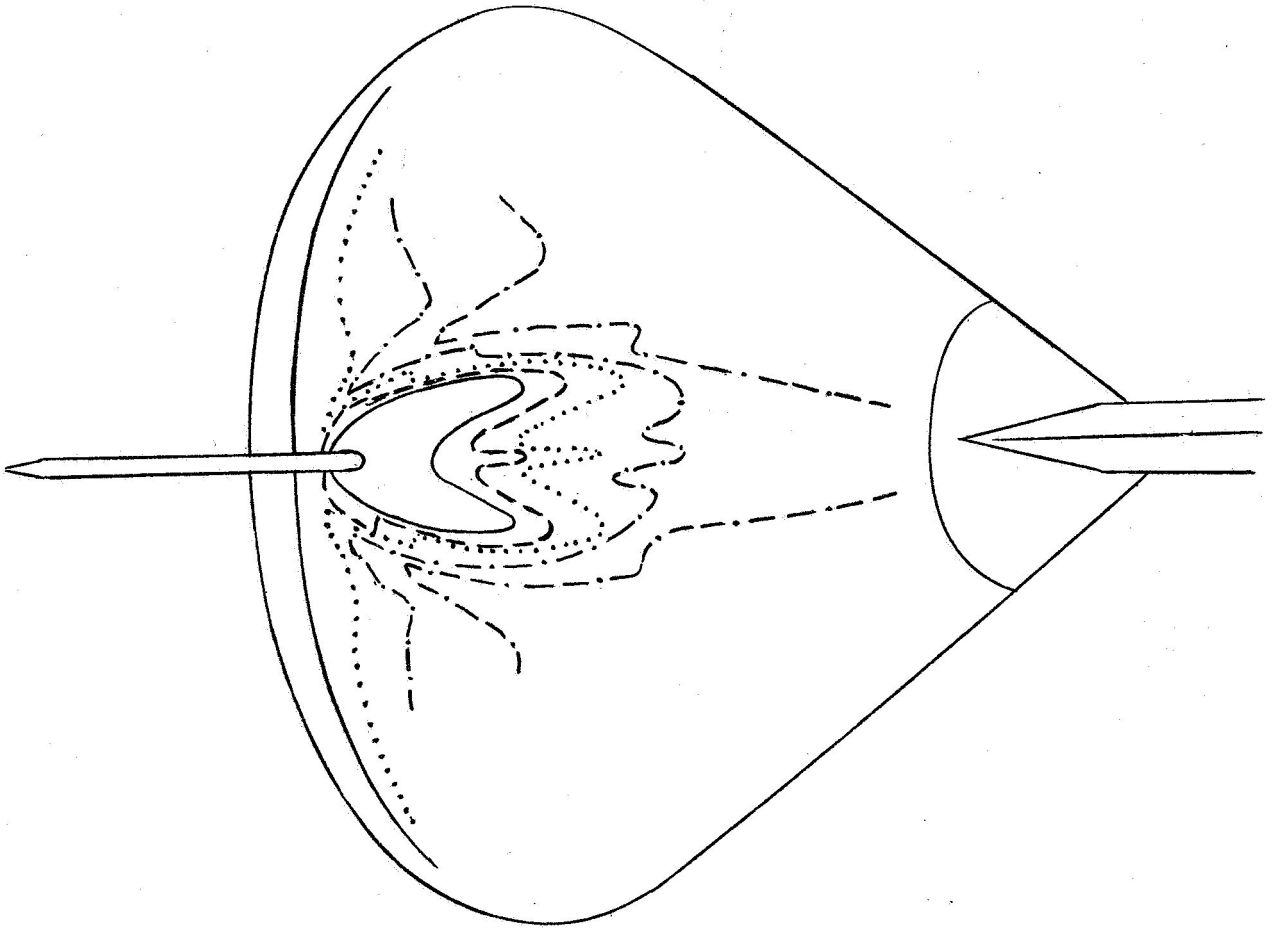

(d) a = 2.39 cm; b = 0.635 cm; c = 1.27 cm; $\theta = 90^0$; blunt leading-edge strut.

Figure 7.- Continued.

L-69-1244

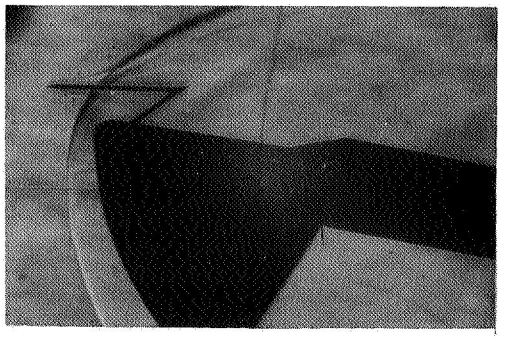

$\frac{h}{h_o}$

0.23 · · · · · · · · · · · · · ·
.18 — · — · — · —
.14 — — · — — · — —

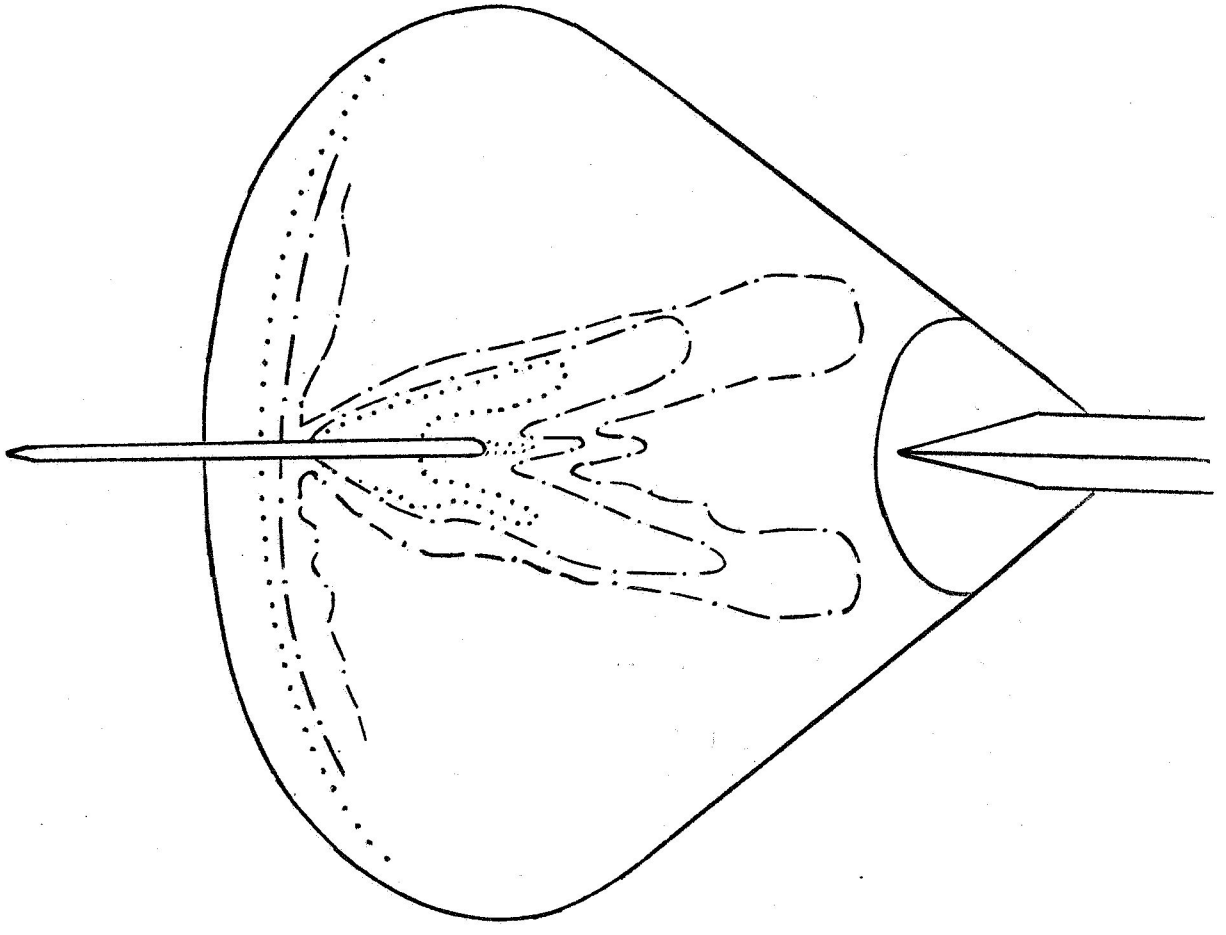

(e) a = 1.27 cm; b = 1.02 cm; c = 1.27 cm; $\theta = 45^{0}$; blunt leading-edge strut.

Figure 7.- Continued.

L-69-1245

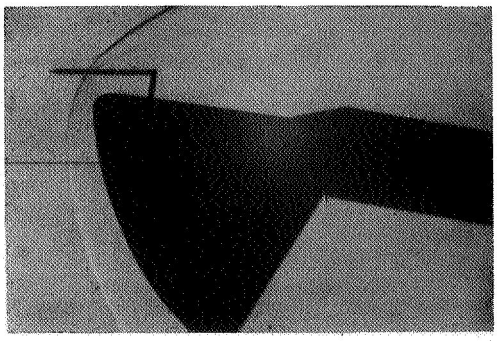

$\frac{h}{h_o}$

0.50 ——————
.32 — — — —
.23 . . . . . .
.18 —·—·—·—
.14 ——·——

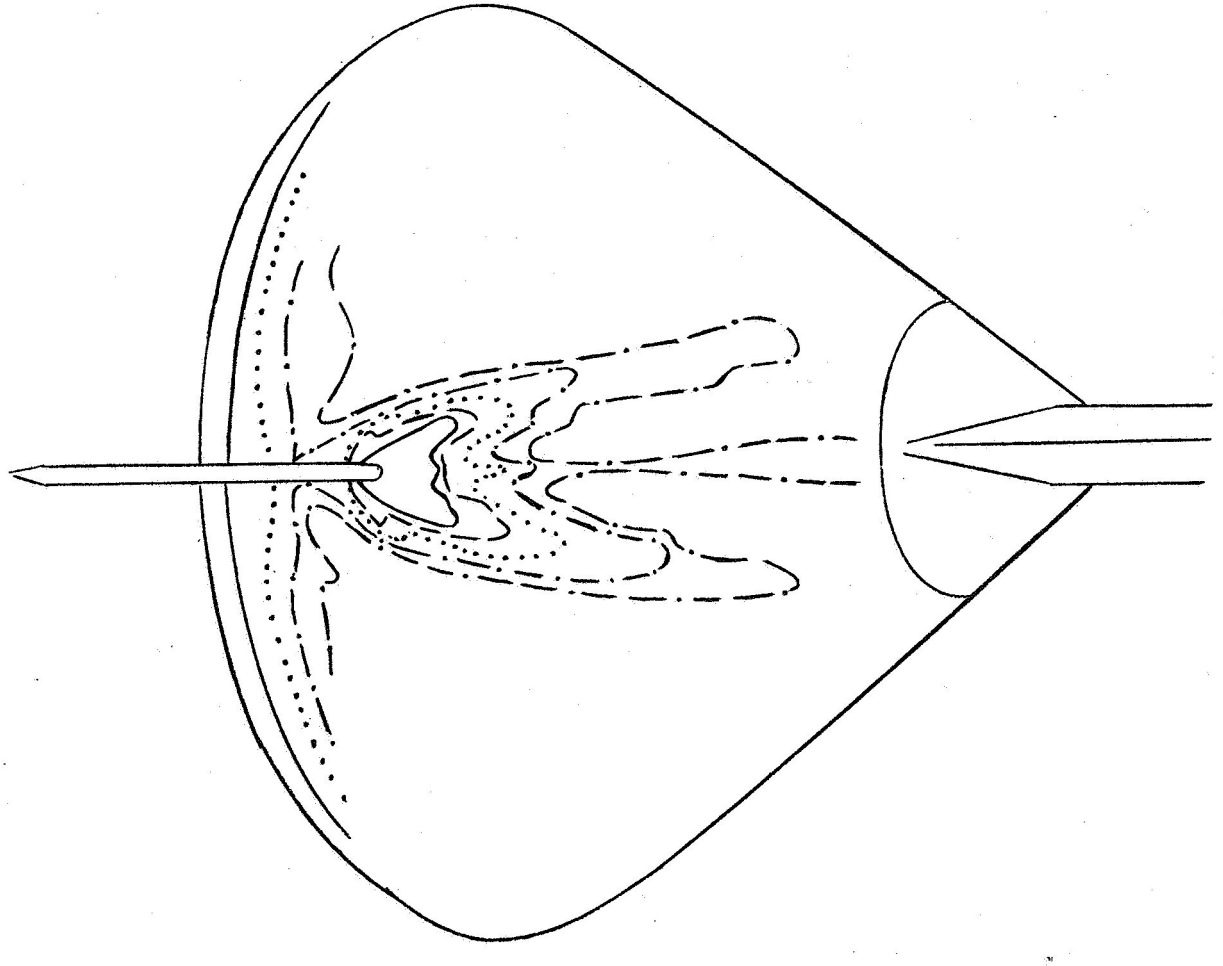

(f) a = 1.27 cm; b = 0.635 cm; c = 2.03 cm; $\theta = 90^{o}$; blunt leading-edge strut.

Figure 7.- Continued.

L-69-1246

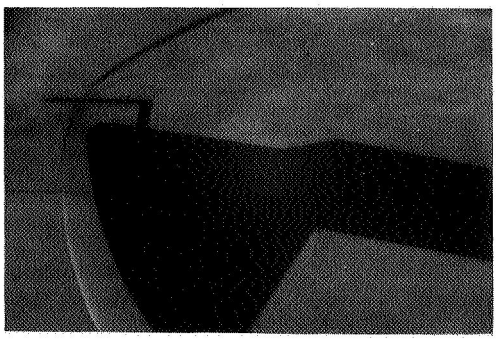

$\frac{h}{h_o}$

0.50 ——————

.32 — — — — —

.23 - - - - - - - - - - - - -

.18 — · — · — · —

.14 — — · — · —

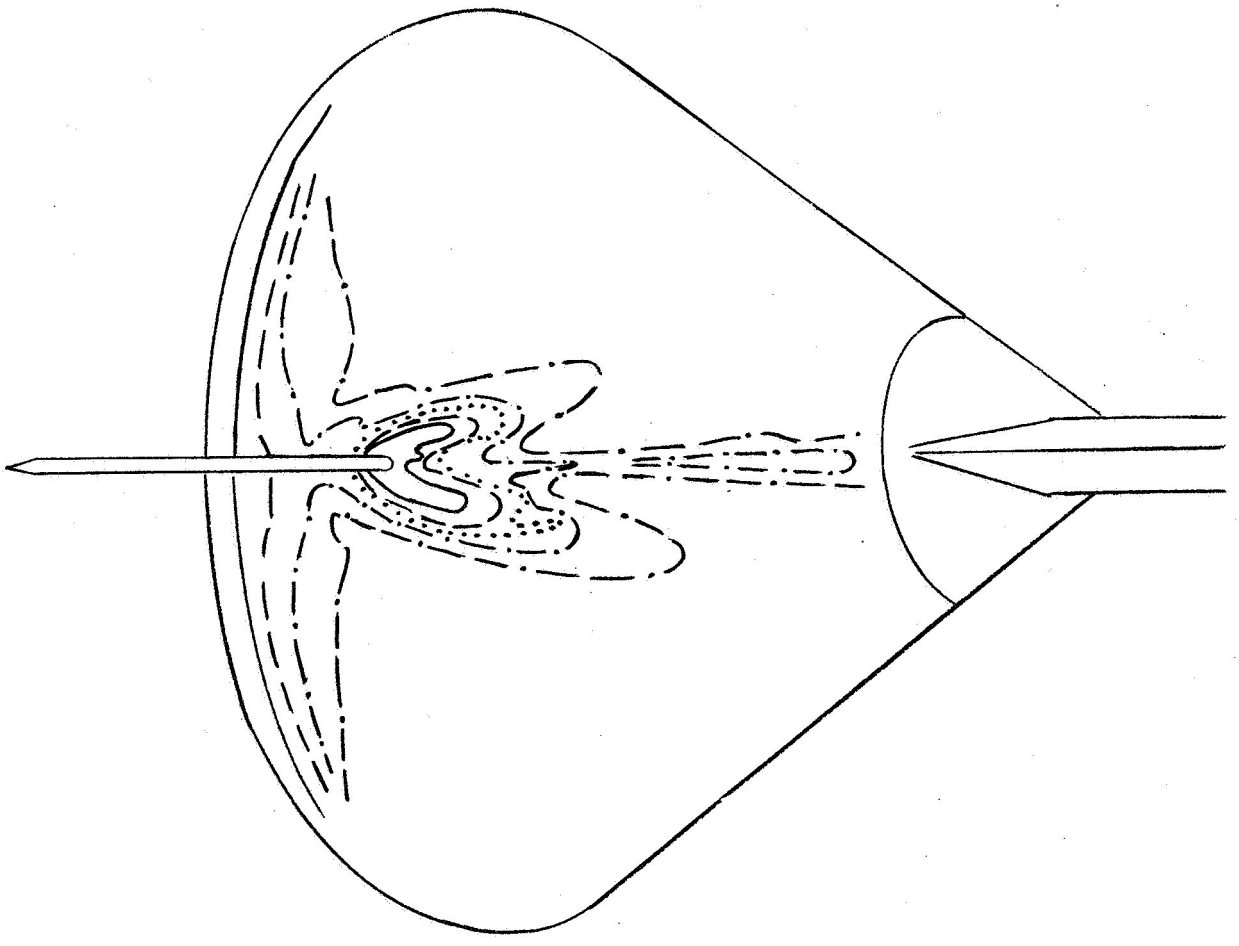

(g) a = 1.27 cm; b = 0.635 cm; c = 2.03 cm; $\theta = 90^{o}$; sharp leading-edge strut.

Figure 7.- Continued. L-69-1247

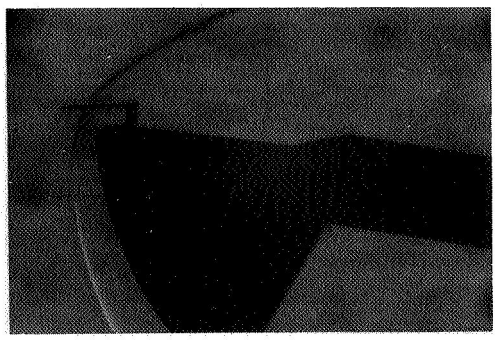

$\frac{h}{h_o}$

0.50 ——————
.32 — — — — —
.23 ·····
.14 — — · — —

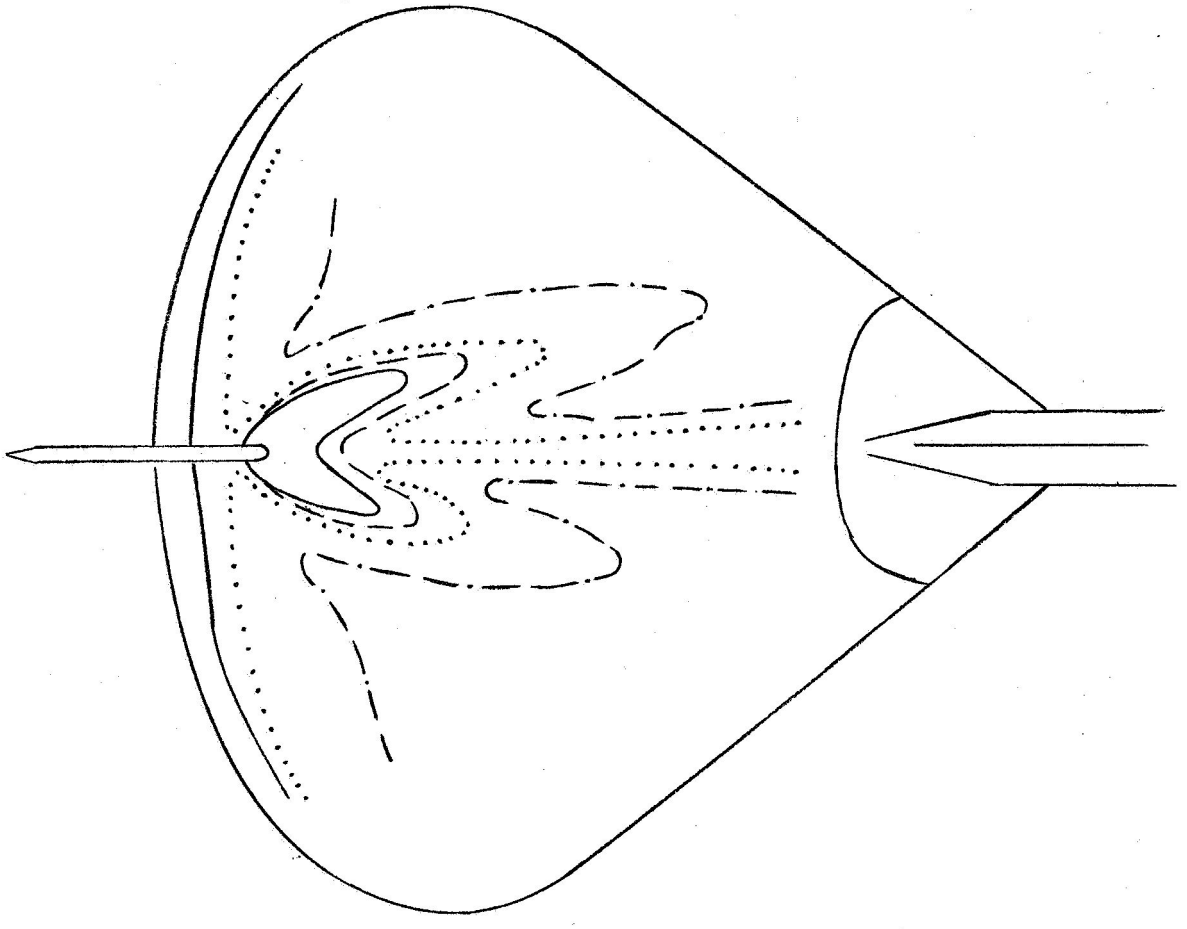

(h) a = 1.27 cm; b = 0.635 cm; c = 1.27 cm; $\theta = 90^{o}$; sharp leading-edge strut.

Figure 7.- Continued. L-69-1248

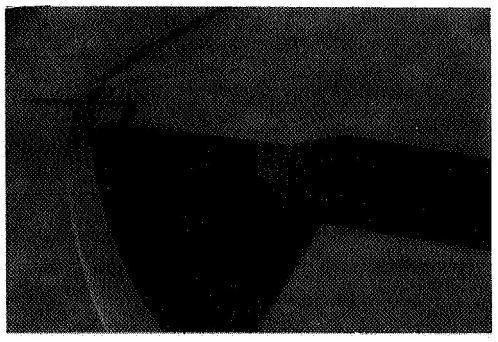

$\frac{h}{h_o}$

0.50 ——————
.32 — — — — —
.23 ----------
.18 —·—·—·—
.14 —··—··—··—

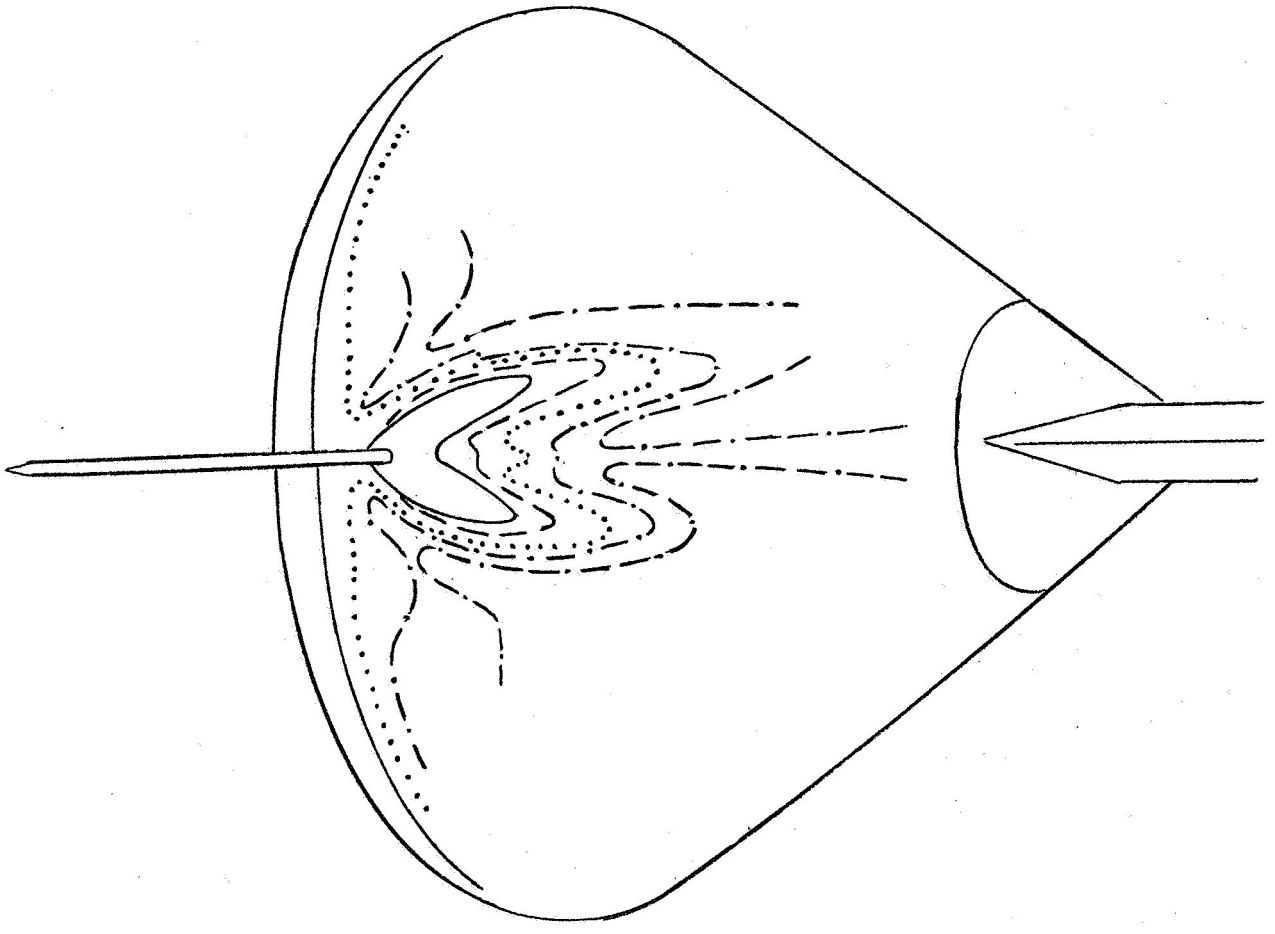

(i) a = 2.39 cm; b = 0.635 cm; c = 1.27 cm; $\theta = 90^{0}$; sharp leading-edge strut.

Figure 7.- Continued. L-69-1249

$\frac{h}{h_o}$

0.32 — — — — —
.23 ·····
.18 — · — · — · —
.14 — — · — —
.11 — · · — · · —

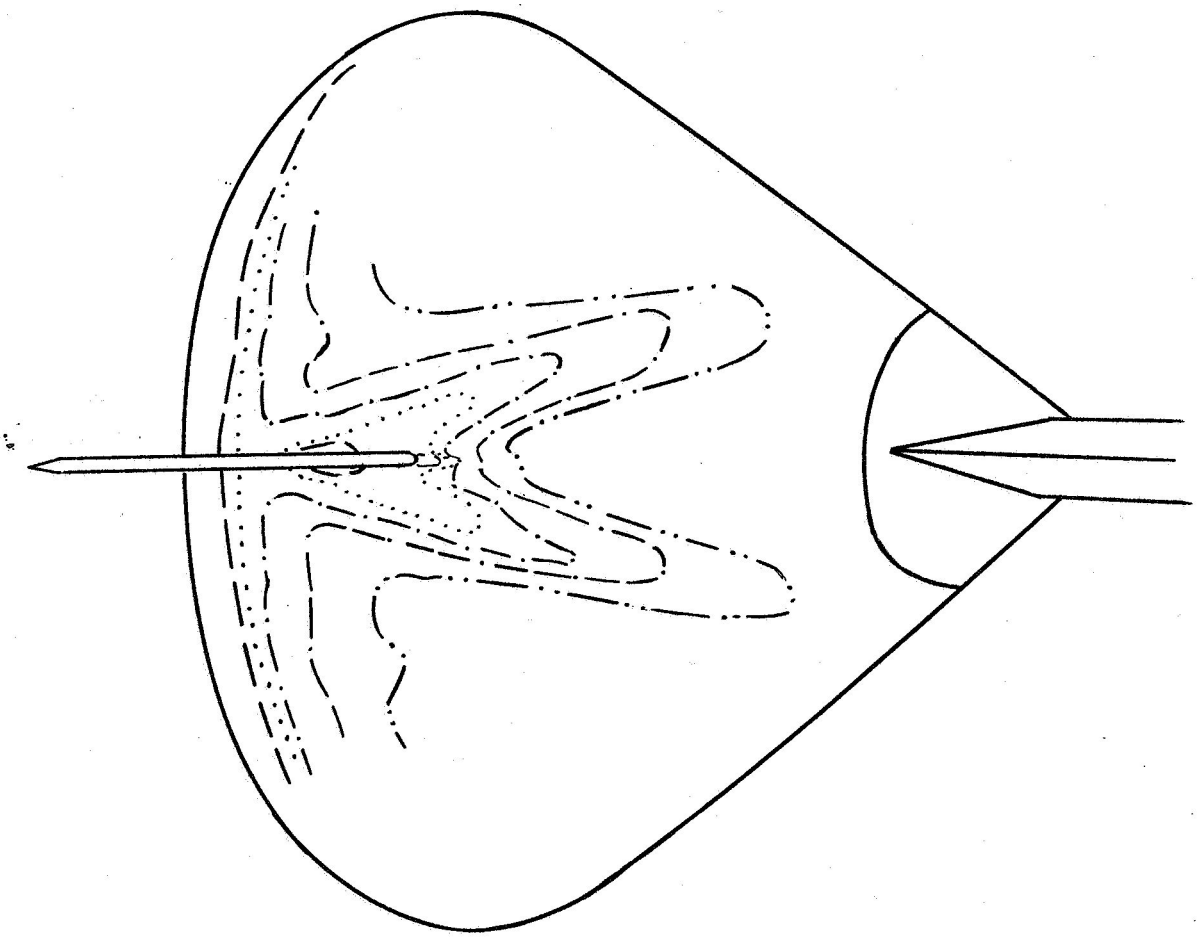

(j) a = 1.27 cm; b = 0.635 cm; c = 1.27 cm; $\theta = 45^0$; fillet.

Figure 7.- Concluded. L-69-1250

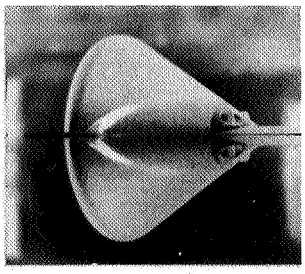

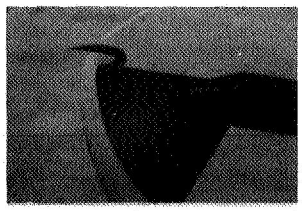

Schlieren photo

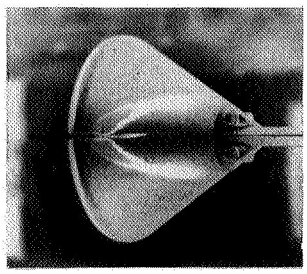

Phase-change coating patterns

$\frac{h}{h_0}$

1.20 ————

.55 — — —

.39 · · · · · ·

.24 — · — · —

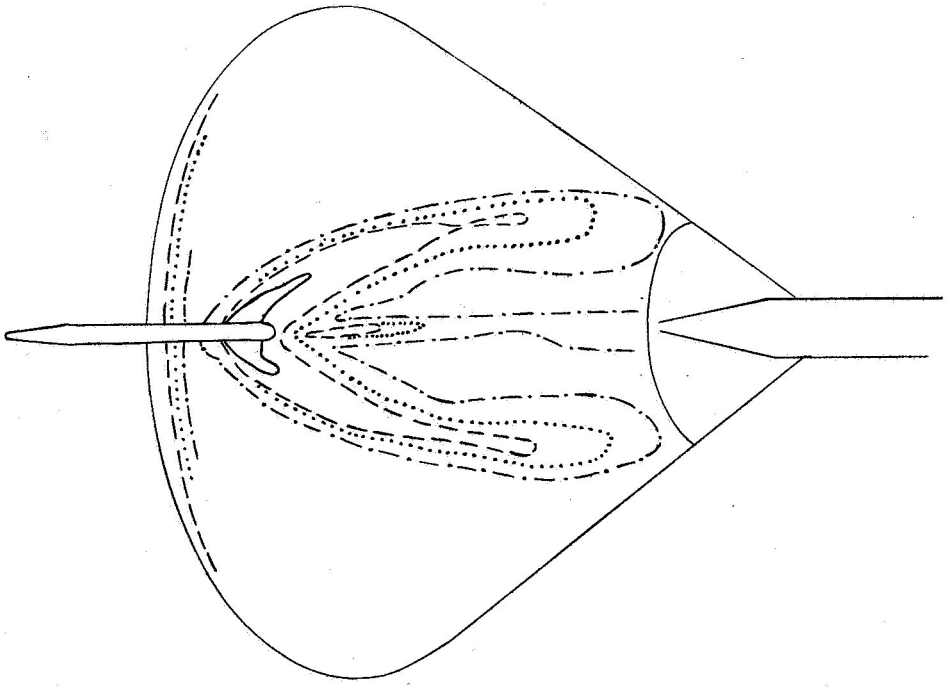

Figure 8.- Interference heating on model with final probe-antenna configuration. $R_{\infty,D} = 0.33 \times 10^6$. L-69-1251

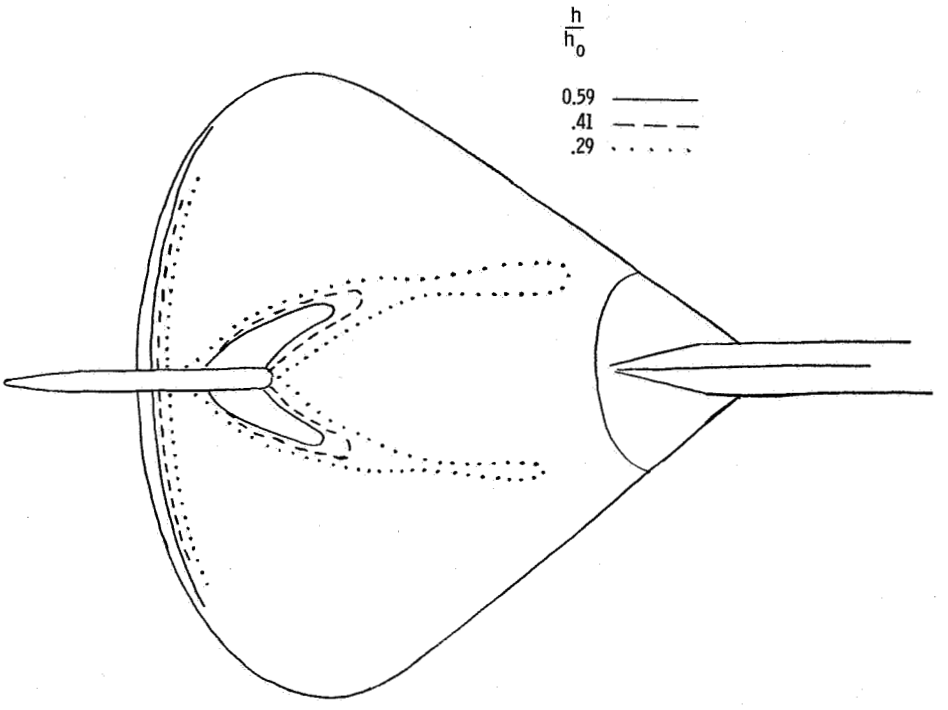

(a) $R_{\infty,D} = 0.23 \times 10^6$.

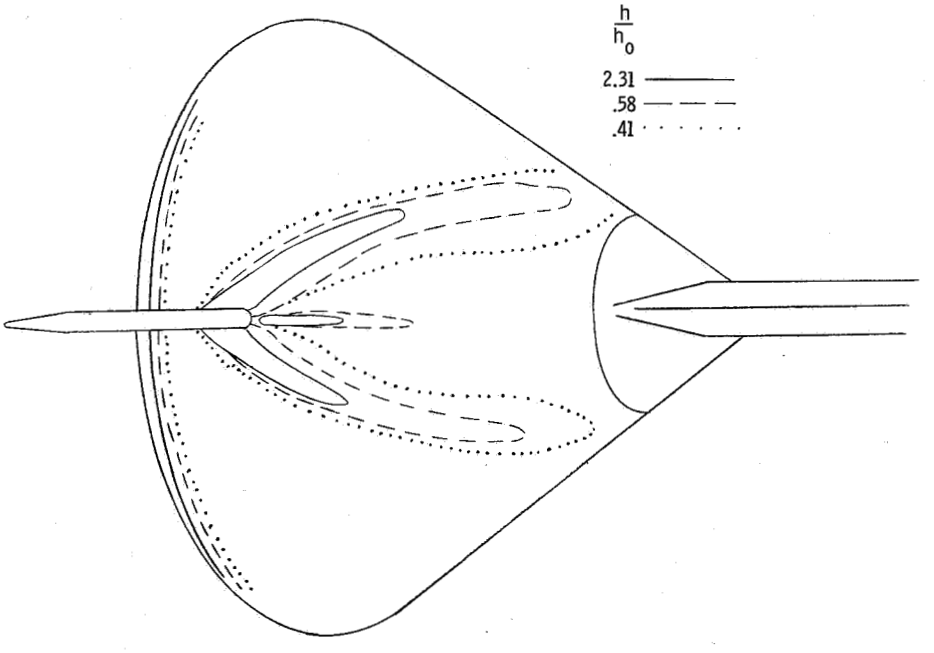

(b) $R_{\infty,D} = 0.51 \times 10^6$.

Figure 9.- Effect of Reynolds number for final probe-antenna configuration.

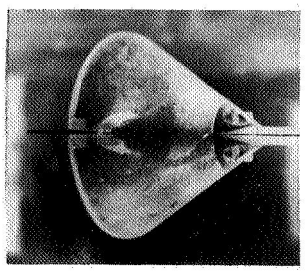

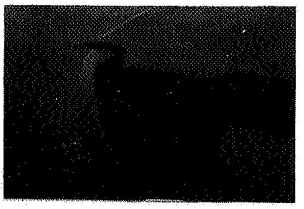

Schlieren photo

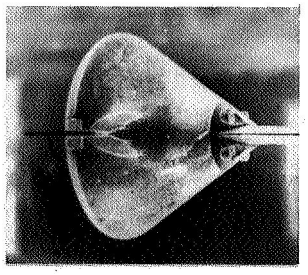

Phase-change coating patterns

$\frac{h}{h_o}$

0.50 — — — —
.35 · · · · · · · · · · · ·
.22 — · — · — ·

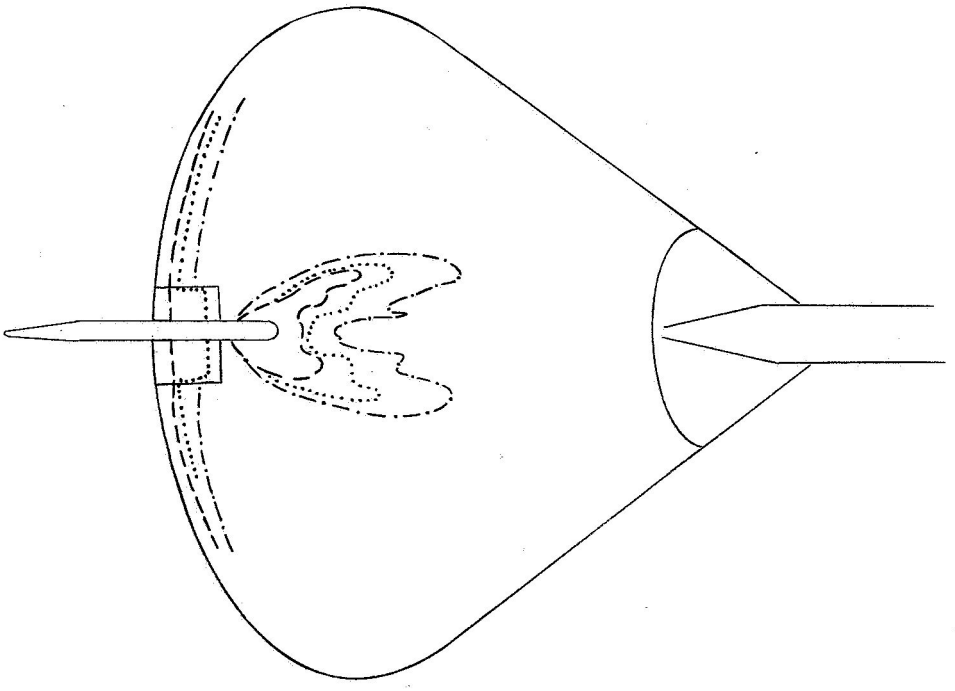

Figure 10.- Effect of ramp on interference heating to afterbody. $R_{\infty,D} = 0.33 \times 10^6$. L-69-1252

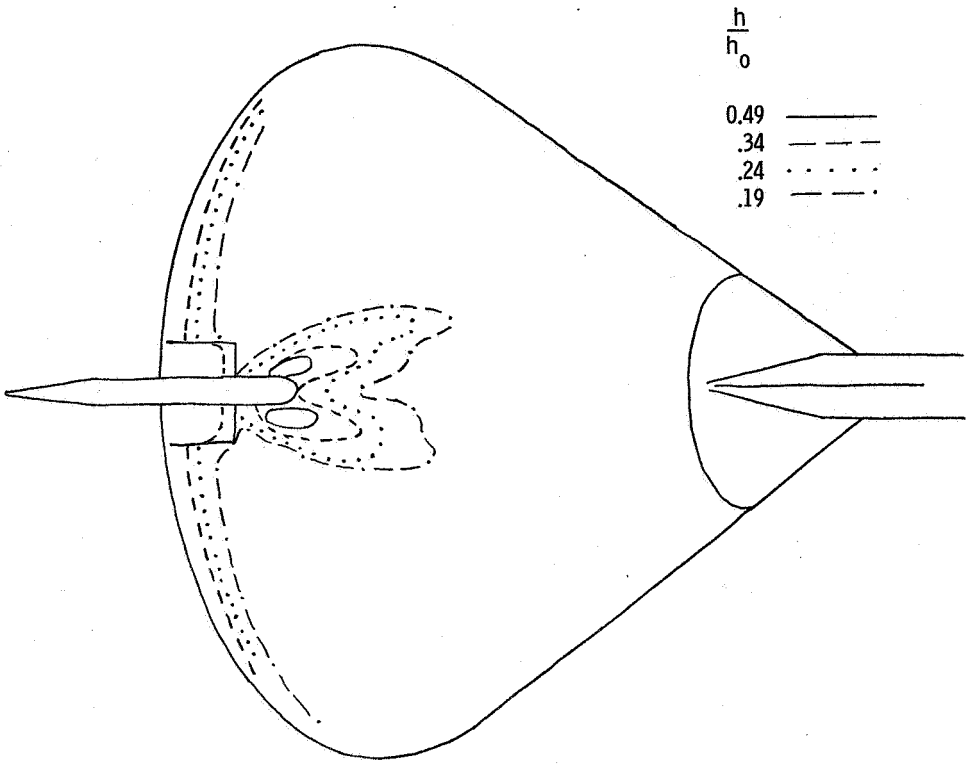

(a) $R_{\infty,D} = 0.23 \times 10^6$.

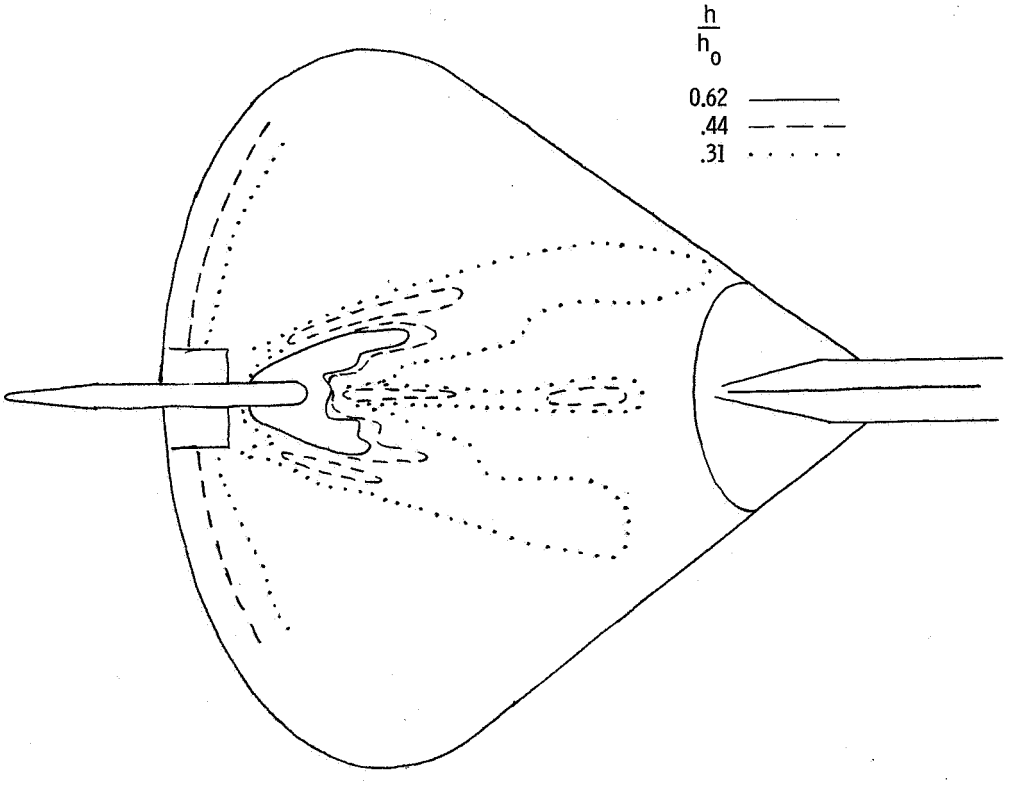

(b) $R_{\infty,D} = 0.51 \times 10^6$.

Figure 11.- Effect of Reynolds number for final probe-antenna configuration with ramp.

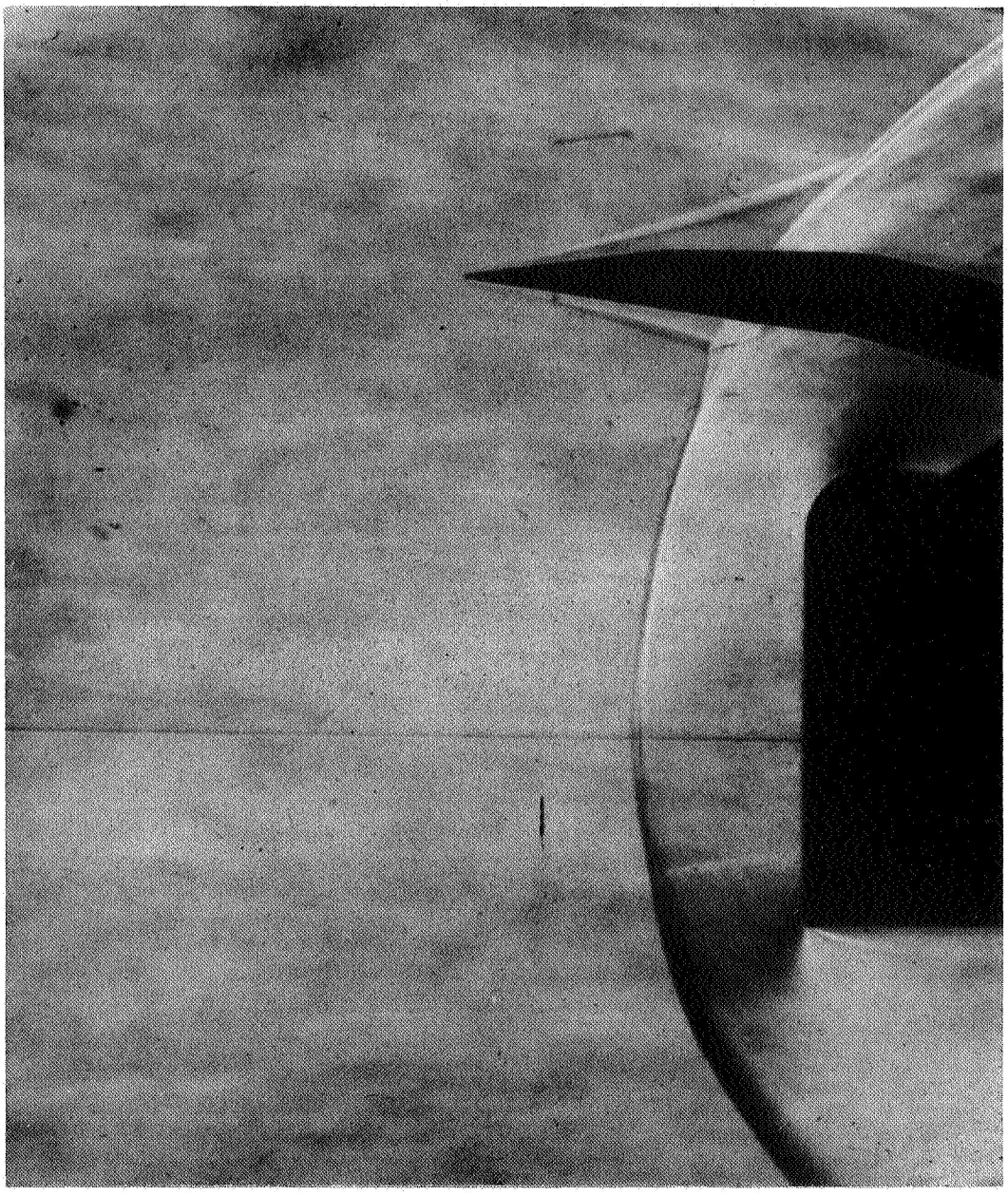

Figure 12.- Flow about probe antenna on two-dimensional model. L-69-1253

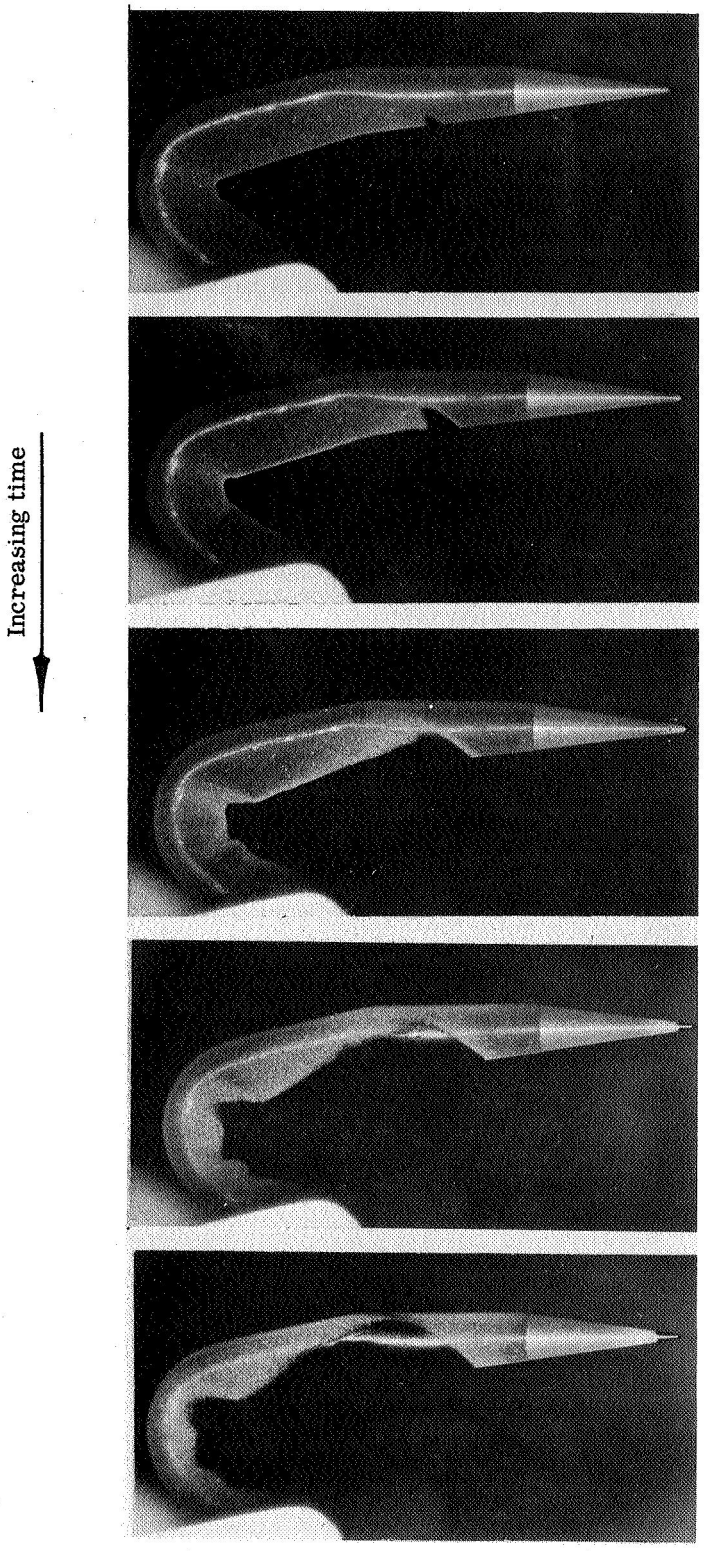

Figure 13.- Phase-change patterns on probe antenna. L-69-1254

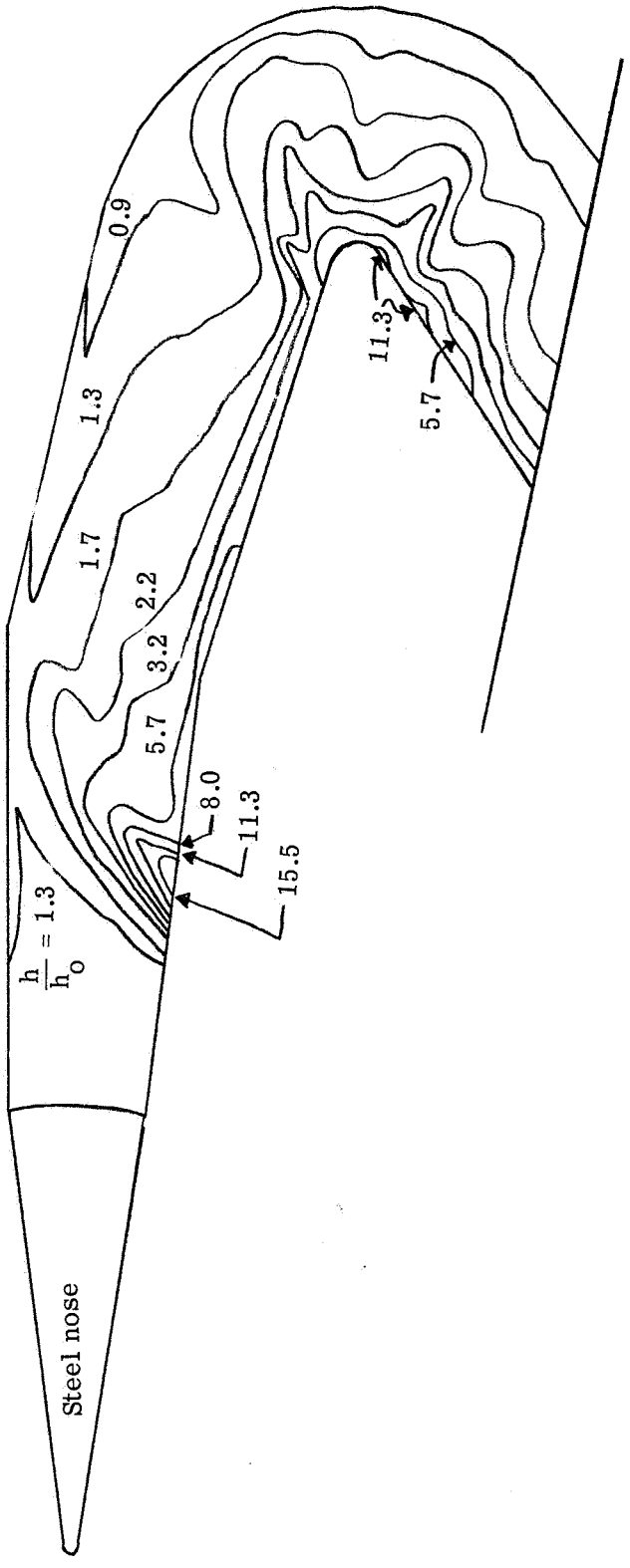

Figure 14.- Interference heating to probe. $r_{n,eff}$ = 37.08 cm; h_o = 98.9 W/m^{2-o}K; $R_{\infty,D}$ = 1.53 × 10^6.

NATIONAL AERONAUTICS AND SPACE ADMINISTRATION
WASHINGTON, D.C. 20546

OFFICIAL BUSINESS

FIRST CLASS MAIL

POSTAGE AND FEES PAID
NATIONAL AERONAUTICS AND
SPACE ADMINISTRATION

POSTMASTER: If Undeliverable (Section 158 Postal Manual) Do Not Return

"The aeronautical and space activities of the United States shall be conducted so as to contribute . . . to the expansion of human knowledge of phenomena in the atmosphere and space. The Administration shall provide for the widest practicable and appropriate dissemination of information concerning its activities and the results thereof."

—NATIONAL AERONAUTICS AND SPACE ACT OF 1958

NASA SCIENTIFIC AND TECHNICAL PUBLICATIONS

TECHNICAL REPORTS: Scientific and technical information considered important, complete, and a lasting contribution to existing knowledge.

TECHNICAL NOTES: Information less broad in scope but nevertheless of importance as a contribution to existing knowledge.

TECHNICAL MEMORANDUMS: Information receiving limited distribution because of preliminary data, security classification, or other reasons.

CONTRACTOR REPORTS: Scientific and technical information generated under a NASA contract or grant and considered an important contribution to existing knowledge.

TECHNICAL TRANSLATIONS: Information published in a foreign language considered to merit NASA distribution in English.

SPECIAL PUBLICATIONS: Information derived from or of value to NASA activities. Publications include conference proceedings, monographs, data compilations, handbooks, sourcebooks, and special bibliographies.

TECHNOLOGY UTILIZATION PUBLICATIONS: Information on technology used by NASA that may be of particular interest in commercial and other non-aerospace applications. Publications include Tech Briefs, Technology Utilization Reports and Notes, and Technology Surveys.

Details on the availability of these publications may be obtained from:

SCIENTIFIC AND TECHNICAL INFORMATION DIVISION

NATIONAL AERONAUTICS AND SPACE ADMINISTRATION

Washington, D.C. 20546